

Identification of Multi-Input Systems in the Presence of Highly-Correlated Inputs

Tom Berger*, Mark B. Tischler†, Marit E. Knapp‡ and Mark J. S. Lopez§

U.S. Army Aviation Development Directorate, Moffett Field, CA, 94035

Frequency-domain identification of multi-input systems with highly-correlated inputs is performed using the Joint Input-Output method. This method allows for highly-correlated inputs by considering both the input and output of the system jointly as the outputs to some uncorrelated (or partially-correlated) reference input. After a brief discussion of multi-input system identification, the Joint Input-Output method is applied to two simulation examples—a business jet model and a compound rotorcraft model both with control systems that result in fully correlated bare-airframe inputs. The results of both simulation examples show that using the Joint Input-Output method recovers the correct bare-airframe frequency responses when compared to the known simulation models. Subsequently, the method is applied to flight data for a business jet with a fly-by-wire control system that fully correlates the bare-airframe inputs. The business jet flight-test results show excellent agreement between closed-loop flight data processed with the Joint Input-Output method and open-loop flight data with no input correlation. Finally, the Joint Input-Output method is used to identify frequency responses of an octocopter UAV to individual motor inputs from flight-test data. The results of the octocopter identification are validated using the known moment arms of the individual motors.

Nomenclature

| | |
|-----------------|--|
| β | Sideslip angle [deg or rad] |
| δ | Vector of inputs |
| C | MIMO controller or mixer |
| F | MIMO feed-forward or prefilter |
| G | Matrix of auto- and cross-spectra |
| H | MIMO feedback or sensor model |
| M | Mixing matrix |
| P | MIMO bare-airframe |
| r | Reference input |
| y | Vector of outputs |
| δ | Single input |
| γ_{xy}^2 | Coherence from input x to output y |
| ω | Frequency [rad/sec] |
| ϕ | Phase angle [deg] |
| G_{xy} | Cross-spectrum |
| j | Imaginary number, $\sqrt{-1}$ |
| p | Roll rate [deg/sec or rad/sec] |
| T | Total record length [sec] |
| t | Time [sec] |

*Aerospace Engineer, U.S. Army Aviation Development Directorate, Senior Member AIAA.

†Senior Technologist, U.S. Army Aviation Development Directorate, Associate Fellow AIAA.

‡Research Associate, San Jose State University Research Foundation, Member AIAA.

§Aerospace Engineer, U.S. Army Aviation Development Directorate, Member AIAA.

Distribution Statement A: Approved for public release; distribution is unlimited.

y Single output

Subscripts

ail Aileron
A Bare-airframe (Actuator)
lat Lateral stick
ped Pedals
rud Rudder
S Pilot (Stick)

I. Introduction

AEROSPACE applications often require the identification of multi-input/multi-output (MIMO) systems, such as a MIMO bare-airframe aircraft model. A non-parametric frequency-response matrix of the different input-output pairs of a MIMO system is necessary for parametric model structure determination and for transfer-function and state-space model identification using frequency-response identification techniques (e.g., Ref. 1). A frequency-response matrix may also be desirable to validate parametric models identified using other frequency- or time-domain identification methods (e.g., Maximum Likelihood Estimate or Output-Error Method²). Many times though, the inputs to these MIMO systems cannot be independently excited and produce off-axis, or secondary, inputs that are correlated with the primary input. Examples of such systems include aircraft with mechanical mixers that cannot be disconnected (such as an aileron-rudder interconnect), aircraft with control allocation that allocate each moment command to multiple bare-airframe inputs, or unstable aircraft that cannot be excited without a control system engaged which feeds back excitations in the primary input to secondary inputs. When the inputs are highly correlated, the effects of each individual input on each output cannot be separated, and an accurate frequency-response model of the MIMO system cannot be determined without some additional processing. This paper reviews and applies the Joint Input-Output (JIO) Method for frequency-response identification with *highly-correlated inputs*.

Several approaches have been proposed to mitigate the issue of correlated inputs. The simplest approach is to perform the identification using a Direct Method, where the bare-airframe input and output data are used directly, either ignoring [*Single-Input/Single-Output (SISO) Direct Method*] or conditioning for [*Multi-Input/Single-Output (MISO) Direct Method*] any potentially correlated secondary inputs. Reference 1 provides a MISO Direct Method to condition the data and remove the effects of partially-correlated secondary inputs, however, the method breaks down for highly- or fully-correlated inputs.

Another approach to mitigate high input-correlation is to de-correlate the inputs by summing random signals uncorrelated with the primary input to the secondary inputs. This was demonstrated successfully while identifying a model of a Bell 206 helicopter from flight data,³ where the copilot randomly pulsed the secondary controls while the pilot performed a frequency sweep in the primary control. An alternative method is to use mutually orthogonal multisine signals for each input simultaneously, which by design attempts to keep the inputs uncorrelated.² Then, SISO frequency responses from each individual input to each output can be extracted at that input's discrete, known input frequencies using a discrete Fourier transform (DFT).^{2,4} This method is referred to herein as the *Orthogonal DFT Method*. However, in the presence of feedback and coupling in either the bare-airframe or the feedback, discrete frequencies in one axis may be fed back to the other axes and render the inputs no longer orthogonal and this method will break down.

When a control system is causing the correlation, nonlinearities (such as a deadband or a conditional controller⁵) can be added to the secondary input channels to reduce the correlation with the primary input. Reference 6 lists two additional approaches for performing bare-airframe identification in the presence of a control system (i.e., closed-loop identification). The first additional approach is called the *Indirect Method* and consists of two steps: 1) Identify the closed-loop system for which the inputs can generally be made uncorrelated or only partially correlated and 2) Extract the bare-airframe model using knowledge of the controller. The main limitation of the Indirect Method is that any errors in knowledge of the controller (e.g., under- or over-estimation of the time delay in the feedback path) will be manifested as errors in the bare-airframe model.⁶ The second approach to closed-loop identification given in Ref. 6 is called the *Joint Input-Output (JIO) Method*, where both the input and output of the bare-airframe are considered jointly as outputs to some uncorrelated (or partially-correlated) reference input.

The JIO Method was proposed by Akaike⁷ as a way to mitigate measurement noise correlation when

analyzing systems with feedback. More recently, the JIO method was utilized by Gennaretti et al.⁸ and Hersey et al.⁹ for identification of rotorcraft inflow models with highly-correlated inputs, and by Knapp et al.¹⁰ to identify a flight dynamics model of an F-16 from closed-loop flight data.

Herein, the JIO Method is utilized to solve the highly-correlated input system-identification problem for flight dynamics models using frequency-domain system-identification techniques.¹ The JIO Method will be used to generate a frequency-response matrix of the different input-output pairs of a MIMO system.

A brief description of the MISO Direct and JIO Methods with application to aircraft identification is provided in Sec. II. Two simulation examples are presented in Sec. III. The first is based on the lateral/directional dynamics of a business jet with a simple control system which results in highly-correlated bare-airframe inputs. Bare-airframe frequency responses are extracted from frequency sweeps input at the actuators using the Direct and JIO Methods, and also from orthogonal multisines input at the actuators using the Orthogonal DFT Method. The results are then compared to the known model. The second simulation example is based on a compound rotorcraft with multiple redundant controls and a control system and control allocation scheme that results in highly-correlated bare-airframe inputs. Bare-airframe frequency responses to individual actuators are extracted from frequency sweeps input at the actuators using the Direct and JIO Methods, and are compared to the known model. In Sec. IV, the JIO Method is first applied to closed-loop flight-test data of a business jet, which contain highly-correlated bare-airframe inputs. Bare-airframe frequency responses are extracted from the flight-test data using both the Direct and JIO Methods, and are compared to frequency responses extracted from open-loop flight data collected with no control system, thereby validating the JIO Method. Then, the JIO Method is used to identify the bare-airframe dynamics of an octocopter unmanned aerial vehicle (UAV) to individual motors, which are highly correlated due to control mixing, from flight-test data. Finally, conclusions are provided in Sec. V.

II. Frequency Response Identification of MIMO Flight Dynamics Models

Consider the generic block diagram shown in Fig. 1, with MIMO bare-airframe \mathbf{P} , controller/mixer \mathbf{C} , feedback/sensor model \mathbf{H} , and feed-forward/prefilter \mathbf{F} . The pilot stick inputs are denoted by vector $\delta_S \in \mathbb{R}^{n_S}$, bare-airframe inputs by vector $\delta_A \in \mathbb{R}^{n_A}$, and bare-airframe outputs by vector $\mathbf{y} \in \mathbb{R}^{n_y}$. Inputs $\delta_{A_{in}} \in \mathbb{R}^{n_A}$ may also be summed directly into the bare-airframe inputs.

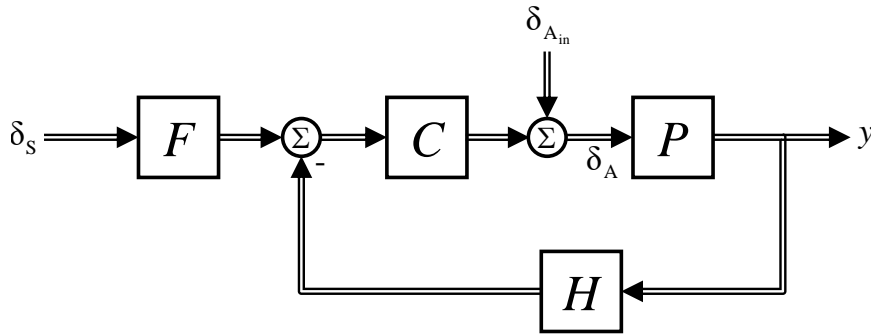


Figure 1. Generic closed-loop block diagram.

The MIMO bare-airframe \mathbf{P} can be expressed as a matrix of frequency responses:

$$\mathbf{P}(j\omega) = \begin{bmatrix} \frac{y_1}{\delta_{A_1}}(j\omega) & \dots & \frac{y_1}{\delta_{A_{n_A}}}(j\omega) \\ \vdots & \ddots & \vdots \\ \frac{y_{n_y}}{\delta_{A_1}}(j\omega) & \dots & \frac{y_{n_y}}{\delta_{A_{n_A}}}(j\omega) \end{bmatrix} \equiv \begin{bmatrix} \mathbf{y} \\ \delta_A \end{bmatrix}(j\omega) \quad (1)$$

which can be identified from flight data by exciting the bare-airframe through some external excitation (e.g., δ_S or $\delta_{A_{in}}$ in Fig. 1), and measuring δ_A and \mathbf{y} .

A. Multi-Input/Single-Output Direct Method

Using the frequency-domain Multi-Input/Single-Output (MISO) Direct Method,¹ the bare-airframe frequency-response matrix $[\mathbf{y}/\boldsymbol{\delta}_A]$ can be identified from the following auto- and cross-spectra quantities:

$$\underbrace{\begin{bmatrix} \frac{y_1}{\delta_{A_1}}(j\omega) & \cdots & \frac{y_1}{\delta_{A_{n_A}}}(j\omega) \\ \vdots & \ddots & \vdots \\ \frac{y_{n_y}}{\delta_{A_1}}(j\omega) & \cdots & \frac{y_{n_y}}{\delta_{A_{n_A}}}(j\omega) \end{bmatrix}}_{\left[\frac{\mathbf{y}}{\boldsymbol{\delta}_A}(j\omega)\right]} = \underbrace{\begin{bmatrix} G_{\delta_{A_1}y_1}(j\omega) & \cdots & G_{\delta_{A_{n_A}}y_1}(j\omega) \\ \vdots & \ddots & \vdots \\ G_{\delta_{A_1}y_{n_y}}(j\omega) & \cdots & G_{\delta_{A_{n_A}}y_{n_y}}(j\omega) \end{bmatrix}}_{\left[\mathbf{G}_{\delta_A y}(j\omega)\right]} \underbrace{\begin{bmatrix} G_{\delta_{A_1}\delta_{A_1}}(j\omega) & \cdots & G_{\delta_{A_{n_A}}\delta_{A_1}}(j\omega) \\ \vdots & \ddots & \vdots \\ G_{\delta_{A_1}\delta_{A_{n_A}}}(j\omega) & \cdots & G_{\delta_{A_{n_A}}\delta_{A_{n_A}}}(j\omega) \end{bmatrix}}_{\left[\mathbf{G}_{\delta_A\delta_A}(j\omega)\right]^{-1}}^{-1} \quad (2)$$

Note that Eq. 2 represents an $n_y \times n_A \times n_\omega$ matrix (i.e., an $n_y \times n_A$ matrix at each of the n_ω frequency points). In CIPHER^{®1} for example, the spectral quantities (G_{xy}) in the right-hand side of Eq. 2 are first extracted from windowed time history data. Then, the calculation in Eq. 2 is applied one output at a time (e.g., y_1 in Eq. 2) to produce conditioned frequency responses. Finally, the conditioned frequency responses from the different windows are combined into composite frequency responses.

When high correlation exists between the bare-airframe inputs $\boldsymbol{\delta}_A$ (e.g., due to controller crossfeeds or bare-airframe coupling), the matrix $\mathbf{G}_{\delta_A\delta_A}(j\omega)$ will be nearly singular and cannot be inverted to complete the calculation in Eq. 2. In fact, Ref. 1 lists a guideline based on the average cross-control coherence $\gamma_{\delta_{A_i}\delta_{A_j}}^2$ between the primary input δ_{A_i} and secondary inputs δ_{A_j} under which the MISO Direct Method may be used:

$$\left(\gamma_{\delta_{A_i}\delta_{A_j}}^2\right)_{\text{ave}} < 0.5 \quad \text{for } i, j = 1, \dots, n_A \text{ and } i \neq j \quad (3)$$

If Eq. 3 is not satisfied, but the average secondary control autospectra $G_{\delta_{A_j}\delta_{A_j}}$ are small compared to the average primary control autospectrum $G_{\delta_{A_i}\delta_{A_i}}$:

$$\left(G_{\delta_{A_j}\delta_{A_j}}\right)_{\text{ave}} - \left(G_{\delta_{A_i}\delta_{A_i}}\right)_{\text{ave}} \leq -20 \text{ dB} \quad \text{for } i, j = 1, \dots, n_A \text{ and } i \neq j \quad (4)$$

then the secondary inputs can be ignored in the analysis,¹ and the MISO Direct Method in Eq. 2 collapses to the SISO Direct Method, given by:

$$\frac{y_i}{\delta_{A_j}}(j\omega) = \frac{G_{\delta_{A_j}y_i}(j\omega)}{G_{\delta_{A_j}\delta_{A_j}}(j\omega)} \quad (5)$$

When neither Eq. 3 nor Eq. 4 are met for the multiple bare-airframe inputs $\boldsymbol{\delta}_A$, then the MISO Direct Method cannot be used and the SISO Direct Method *will yield incorrect results*, as demonstrated in the examples in Sec. III and Sec. IV. For these cases, the MISO Direct Method can be applied using the uncorrelated (or only partially-correlated) external excitations ($\boldsymbol{\delta}_S$ or $\boldsymbol{\delta}_{A_{\text{in}}}$ in Fig. 1) as the inputs, and a post-processing step using the JIO Method is added, as explained next.

B. Joint Input-Output Method

The JIO Method recovers the uncorrelated frequency responses that make up $[\mathbf{y}/\boldsymbol{\delta}_A]$ when the bare-airframe inputs $\boldsymbol{\delta}_A$ are highly correlated. The JIO Method relies on the fact that when performing system identification of MIMO systems, the inputs cannot be highly correlated, however the outputs can. Therefore, if the inputs to the bare-airframe $\boldsymbol{\delta}_A$ are treated as outputs to a set of uncorrelated (or partially-correlated) reference inputs \mathbf{r} , then the correlation in $\boldsymbol{\delta}_A$ is not prohibitive to identifying a MIMO bare-airframe model. Using the JIO Method, the transfer-function matrix representing the bare-airframe can be calculated as:

$$\left[\frac{\mathbf{y}}{\boldsymbol{\delta}_A}(j\omega)\right] = \left[\frac{\mathbf{y}}{\mathbf{r}}(j\omega)\right] \left[\frac{\boldsymbol{\delta}_A}{\mathbf{r}}(j\omega)\right]^{-1} \quad (6)$$

Note that frequency responses matrices $[\mathbf{y}/\mathbf{r}]$ and $[\boldsymbol{\delta}_A/\mathbf{r}]$ in Eq. 6 are extracted from flight data using the MISO Direct Method (Eq. 2) with \mathbf{r} as the input instead of $\boldsymbol{\delta}_A$. Therefore, the reference signal \mathbf{r} must adhere to the guidelines in Eqs. 3 and 4 with the additional restriction:

1. Reference input \mathbf{r} must have the same number of elements as δ_A (i.e., $\mathbf{r} \in \mathbb{R}^{n_A}$), such that the matrix $[\delta_A/\mathbf{r}]$ is square.
2. The independent inputs $r_i, i = 1, \dots, n_A$ that make up \mathbf{r} can be excited independently (i.e., the cross-spectra $G_{r_i r_j}$ are small for all $i \neq j$).
3. The independent inputs $r_i, i = 1, \dots, n_A$ must generate independent combinations of bare-airframe inputs δ_A , such that the matrix $[\delta_A/\mathbf{r}]$ is invertible.

The usual considerations of input noise and correlated feedback of output noise¹ must still be taken into account when selecting the reference signal \mathbf{r} . Signals external to the system (e.g., δ_S or $\delta_{A_{in}}$ in Fig. 1) are the best choice because they can typically be measured with little noise and have no output noise correlation.

For conventional aircraft, typically $n_S = n_A$, and pilot inputs δ_S are a good choice for the uncorrelated (or partially-correlated) reference signals \mathbf{r} . Then, Eq. 6 becomes:

$$\begin{bmatrix} \mathbf{y} \\ \delta_A \end{bmatrix} = \begin{bmatrix} \mathbf{y} \\ \delta_S \end{bmatrix} \begin{bmatrix} \delta_A \\ \delta_S \end{bmatrix}^{-1} \quad (7)$$

When there are redundant bare-airframe controls (i.e., $n_A > n_S$), then $\delta_{A_{in}}$, an external input signal summed into the actuator commands generated by the controller C , is a good choice for \mathbf{r} and Eq. 6 becomes:

$$\begin{bmatrix} \mathbf{y} \\ \delta_A \end{bmatrix} = \begin{bmatrix} \mathbf{y} \\ \delta_{A_{in}} \end{bmatrix} \begin{bmatrix} \delta_A \\ \delta_{A_{in}} \end{bmatrix}^{-1} \quad (8)$$

When $\delta_{A_{in}}$ is the reference input, an automated frequency sweep can be summed into the command of each individual bare-airframe input (e.g., aerosurface actuators for a conventional airplane, swashplate servos for a helicopter, or electric motors for a multi-rotor eVTOL aircraft) one at a time.

Alternatively, the reference input \mathbf{r} can be mixed using a mixing matrix $M \in \mathbb{R}^{n_A \times n_A}$ before generating the external actuator command inputs $\delta_{A_{in}}$, as shown in Fig. 2. Note that the mixing matrix M does not have to be the same as any mixing in the controller C . This allows commanding ganged sets of bare-airframe actuators to only excite certain aircraft responses per input, providing increased transparency of responses to each excitation and more flexibility to fine tune desired responses. One example of this is mixing the reference signal to excite a helicopter swashplate plate in collective, lateral cyclic, and longitudinal cyclic instead of exciting the three swashplate servos individually. Another example is exciting opposite pairs of electric motors of a multi-rotor eVTOL aircraft in a symmetric and differential manner. In both cases, Eq. 6 is applied directly with \mathbf{r} in Fig. 2 as the reference input.

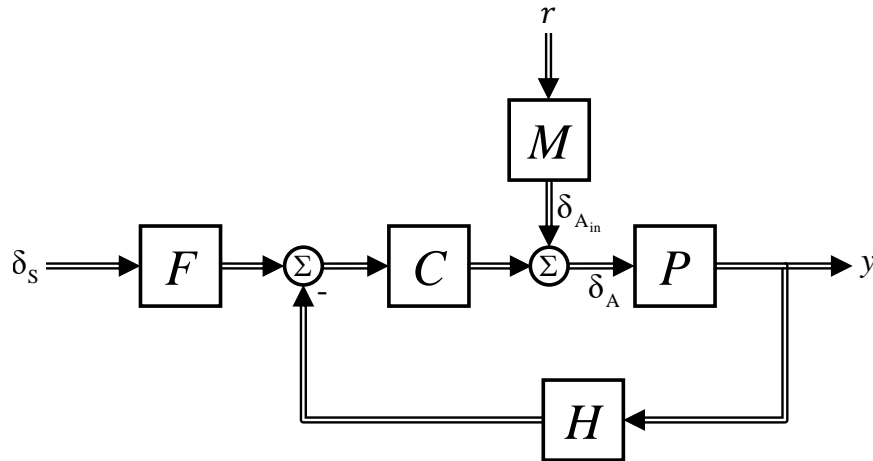


Figure 2. Generic closed-loop block diagram with mixed reference signal.

In all cases of Eqs. 6 through 8, all frequency responses in the matrices on the right hand side of the equations are for inputs with correlation less than the guidelines given in Eqs. 3 and 4, even if the inputs to

the bare-airframe δ_A are highly correlated. Therefore, the JIO Method solves the problems associated with identification of MIMO systems in the presence of highly-correlated inputs. Note that unlike the Indirect Method, the JIO Method does not require any knowledge of \mathbf{F} , \mathbf{C} , or \mathbf{H} in Fig. 1 or \mathbf{M} in Fig. 2 to extract a model of the bare-airframe \mathbf{P} from closed-loop data.

Finally, it is important to assess the quality of the frequency responses generated by the JIO Method for their use in identification of a parametric model using coherence $\gamma_{\delta_{A_i} y_j}^2$. A method to reconstruct the coherence of the frequency responses generated by the JIO Method (elements of $[\mathbf{y}/\delta_A]$) from the coherence of the individual frequency responses used (elements of $[\mathbf{y}/\mathbf{r}]$ and $[\delta_A/\mathbf{r}]$) was developed in Ref. 9. This method is adopted herein with one modification, based on the authors' experience applying the JIO Method to flight-test data, to better represent the quality of the JIO Method frequency responses. Where Ref. 9 assumed the coherence of two multiplied frequency responses H_1 and H_2 , given by $\gamma_{H_1 \times H_2}^2$, is simply equal to the minimum of the two coherences, here it is taken as a *weighted minimum*:

$$\gamma_{H_1 \times H_2}^2 = W(x) \min(\gamma_{H_1}^2, \gamma_{H_2}^2) \quad (9)$$

where:

$$W(x) = [1.582(1 - e^{-x})]^2 \quad (10)$$

$$x = \begin{cases} (\gamma_{H_1}^2 \times \gamma_{H_2}^2)^{1/2} & \text{if } \max(\gamma_{H_1}^2, \gamma_{H_2}^2) < 0.9 \\ y + (1 - y)(\gamma_{H_1}^2 \times \gamma_{H_2}^2)^{1/2} & \text{otherwise} \end{cases} \quad (11)$$

$$y = 10[\max(\gamma_{H_1}^2, \gamma_{H_2}^2) - 0.9] \quad (12)$$

The coherence weighting function $W(x)$ in Eq. 10 is the same as used by Ref. 1, where x in Eq. 11 is the geometric mean when both coherences are below 0.9. If a single coherence is at or above 0.9, then x is interpolated between 1 and the geometric mean using Eq. 12. This interpolation guarantees that the coherence of a product collapses to the minimum coherence when a single coherence is very high. For example, if one of the factors is perfectly known, then the maximum coherence is 1, resulting in $W(x) = x = 1$ and $\gamma_{H_1 \times H_2}^2 = \min(\gamma_{H_1}^2, \gamma_{H_2}^2)$. This can happen when the reference signal is chosen as the actuator signal in the JIO Method.

The JIO Method with coherence calculation presented here will be integrated into the next major release of the CIPHER[®] software tool and will be available by the end of 2019.

III. Simulation Examples

In this section, the JIO Method is applied to simulation data. This allows validation of the JIO identification results against a known bare-airframe model. The first simulation example is of the lateral/directional dynamics of a fixed-wing business jet with two correlated bare-airframe inputs (ailerons and rudder). The second simulation example is of a notional high-speed compound rotorcraft with 10 correlated bare-airframe inputs.

A. Learjet LJ-25D

The simulation example presented here is based on a lateral/directional bare-airframe model of a Learjet LJ-25D (shown in Fig. 3). The bare-airframe model \mathbf{P} was identified from flight-test data at a flight condition of 250 kts (KCAS), 15,000 ft,¹¹ and is given in state-space form as:

$$\begin{aligned} \begin{bmatrix} \dot{v} \\ \dot{p} \\ \dot{r} \\ \dot{\phi} \end{bmatrix} &= \begin{bmatrix} Y_v & Y_p + W_0 & Y_r - U_0 & g \cos \Theta_0 \\ L_v & L_p & L_r & 0 \\ N_v & N_p & N_r & 0 \\ 0 & 1 & \tan \Theta_0 & 0 \end{bmatrix} \begin{bmatrix} v \\ p \\ r \\ \phi \end{bmatrix} + \begin{bmatrix} Y_{\delta_{ail}} & Y_{\delta_{rud}} \\ L_{\delta_{ail}} & L_{\delta_{rud}} \\ N_{\delta_{ail}} & N_{\delta_{rud}} \\ 0 & 0 \end{bmatrix} \begin{bmatrix} \delta_{ail} \\ \delta_{rud} \end{bmatrix} \\ \begin{bmatrix} p \\ \beta \\ \dot{\beta} \end{bmatrix} &= \begin{bmatrix} 0 & 1 & 0 & 0 \\ \frac{1}{V_{tot}} & 0 & 0 & 0 \\ Y_v & Y_p + W_0 & Y_r - U_0 & g \cos \Theta_0 \\ \frac{Y_v}{V_{tot}} & \frac{Y_p + W_0}{V_{tot}} & \frac{Y_r - U_0}{V_{tot}} & \frac{g \cos \Theta_0}{V_{tot}} \end{bmatrix} \begin{bmatrix} v \\ p \\ r \\ \phi \end{bmatrix} + \begin{bmatrix} 0 & 0 \\ 0 & 0 \\ \frac{Y_{\delta_{ail}}}{V_{tot}} & \frac{Y_{\delta_{rud}}}{V_{tot}} \end{bmatrix} \begin{bmatrix} \delta_{ail} \\ \delta_{rud} \end{bmatrix} \end{aligned} \quad (13)$$

Stability and control derivative and trim values are given in Table 1.



Figure 3. Calspan Variable Stability System Learjet LJ-25D.

A notional control system was developed to investigate bare-airframe frequency response identification from closed-loop data. The control system (shown in block diagram form in Fig. 4) consists of a yaw damper using sideslip rate feedback (K_{β}) and an aileron-rudder interconnect (ARI) given by $K_{ARI} = -N_{\delta_{ail}}/N_{\delta_{rud}}$. Control system parameter values are also given in Table 1. The yaw-damper loop has a crossover frequency of $\omega_c = 3.4$ rad/sec, which is typical for a directional controller.¹²

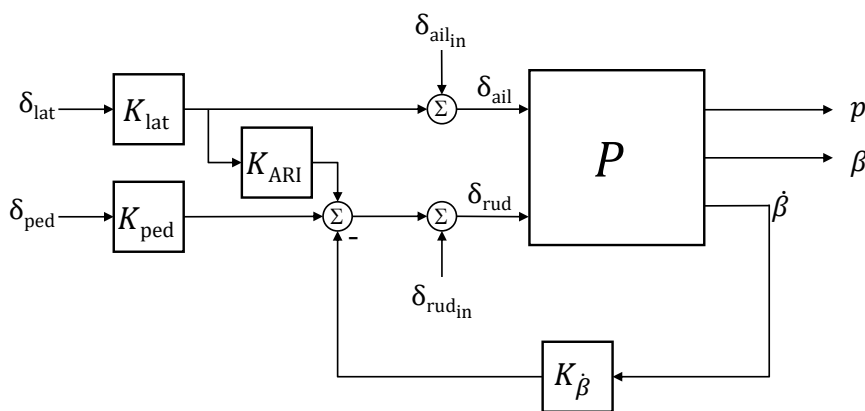


Figure 4. Block diagram of simple LJ-25 lateral/directional control system.

For this idealized example, there are no nonlinearities, actuator or sensor models, time delays, or process or measurement noise. Thus any errors in the identified bare-airframe frequency responses from closed-loop data are attributed to the correlated bare-airframe inputs. Furthermore, since there is no feedback or feed-forward coupling to the ailerons, the aileron input will not be correlated to the rudder input when the rudder is excited. Therefore, we expect all identified frequency responses to rudder inputs (i.e., p/δ_{rud} and β/δ_{rud}) to be accurate, and frequency responses to aileron inputs (i.e., p/δ_{ail} and β/δ_{ail}) to be inaccurate using a Direct Method approach.

Two Learjet simulation examples will be shown. In the first example, bare-airframe frequency responses will be extracted from two time histories: 1) Frequency sweep of the aileron command external input ($\delta_{ail_{in}}$ in Fig. 4) and 2) Frequency sweep of the rudder command external input ($\delta_{rud_{in}}$ in Fig. 4). In the second example, bare-airframe frequency responses will be extracted from a single time history consisting of orthogonal phase-optimized multisine inputs at the aileron and rudder command external inputs simultaneously. The results for both examples are presented together and compared.

Table 1. Learjet Simulation Example Parameter Values (250 kts, 15,000 ft)

| Parameter | Value | Units | Parameter | Value | Units |
|--------------------|---------|---------------------------|--------------------|---------|---------------------------|
| Y_v | -0.1698 | 1/sec | $L_{\delta_{rud}}$ | 0.0330 | rad/sec ² -deg |
| Y_p | 0.8673 | ft/sec-rad | $N_{\delta_{ail}}$ | -0.0113 | rad/sec ² -deg |
| Y_r | 0 | ft/sec-rad | $N_{\delta_{rud}}$ | -0.0373 | rad/sec ² -deg |
| L_v | -0.0192 | rad/sec-ft | U_0 | 536.18 | ft/sec |
| L_p | -2.2776 | 1/sec | W_0 | 20.86 | ft/sec |
| L_r | 0.8487 | 1/sec | V_{tot} | 536.59 | ft/sec |
| N_v | 0.0053 | rad/sec-ft | Θ_0 | 0.039 | rad |
| N_p | -0.2258 | 1/sec | K_{lat} | 5.0 | deg/in |
| N_r | -0.2719 | 1/sec | K_{ped} | 6.0 | deg/in |
| $Y_{\delta_{ail}}$ | -0.0132 | ft/sec ² -deg | K_{ARI} | -0.3020 | deg/deg |
| $Y_{\delta_{rud}}$ | 0.3073 | ft/sec ² -deg | $K_{\dot{\beta}}$ | 1.0 | deg/deg/sec |
| $L_{\delta_{ail}}$ | -0.1623 | rad/sec ² -deg | | | |

1. Frequency Sweep Inputs

Figures 5 and 6 show time histories of the roll- and yaw-axis frequency sweeps input directly into the aileron and rudder actuator commands, respectively ($\delta_{A_{in}} = [\delta_{ail_{in}} \delta_{rud_{in}}]^T$). The total sweep length is $T = 60$ sec for each maneuver, including 5 sec of trim data at the beginning and end of the maneuver. The range of frequencies excited during the sweep is $\omega = 0.8 - 15$ rad/sec. For each maneuver, a sweep amplitude of ± 1.2 deg was used on the swept input, while ± 0.008 deg white noise was added to the non-swept input to mimic flight test conditions where a pure zero signal would not be recorded. Therefore, for each frequency sweep maneuver, the external actuator command inputs $\delta_{A_{in}}$ are not correlated by design.

Figures 5 and 6 also show the bare-airframe inputs aileron and rudder deflections ($\delta_A = [\delta_{ail} \delta_{rud}]^T$) and the bare-airframe outputs ($\mathbf{y} = [p \beta]^T$) for both roll- and yaw-axis frequency sweeps, respectively. During the roll-axis frequency sweep (Fig. 5), the control system produced rudder deflections (secondary input) that are correlated with the aileron deflections (primary input) due to the aircraft coupling β/δ_{ail} , as seen in the fourth subplot in Fig. 5. In contrast, during the yaw-axis frequency sweeps (Fig. 6), the aileron deflection (secondary input) are essentially zero and not correlated with the rudder deflections (primary input), as seen in the third subplot in Fig. 6.

For both frequency sweeps, roll rate p and sideslip β are excited due to bare-airframe coupling, as seen in the bottom two subplots of Figs. 5 and 6.

A quantitative cross-control correlation analysis was performed to confirm the bare-airframe input correlation for the roll-axis sweep seen qualitatively from the time histories in Fig. 5. Figure 7 shows the cross-control correlation analysis for the roll-axis sweep between the bare-airframe inputs (primary input δ_{ail} and secondary input δ_{rud}) and between the external actuator command inputs (primary input $\delta_{ail_{in}}$ and secondary input $\delta_{rud_{in}}$). For the bare-airframe inputs (Fig. 7, solid blue line), the cross-control coherence is $\gamma_{\delta_{ail}\delta_{rud}}^2 \approx 1.0$ over a broad frequency range, violating the guideline in Eq. 3. Therefore, traditional conditioning of the responses using the MISO Direct Method identification technique cannot be used in this case due to the inversion of the ill-conditioned matrix in Eq. 2. One approach is to ignore the secondary input and process the data using the SISO Direct Method. However, as will be shown, this approach will produce the wrong results, since the secondary input magnitude is large compared to the primary input magnitude (Fig. 7, top plot, solid blue line) which violates the guideline in Eq. 4.

In contrast, for the external actuator command input (Fig. 7, dashed red line), the cross-control coherence and secondary input magnitude are low (i.e., meet the guidelines in Eqs. 3 and 4). Therefore, the MISO Direct Method can be applied to the data with the external actuator commands as the inputs ($\mathbf{r} = \delta_{A_{in}} = [\delta_{ail_{in}} \delta_{rud_{in}}]^T$) to extract $[\mathbf{y}/\delta_{A_{in}}]$ and $[\delta_A/\delta_{A_{in}}]$. Then, the JIO Method is applied to post process the results and extract the bare-airframe frequency responses $[\mathbf{y}/\delta_A]$ as in Eq. 8.

The results of the quantitative cross-control correlation analysis for the yaw-axis sweep are shown in

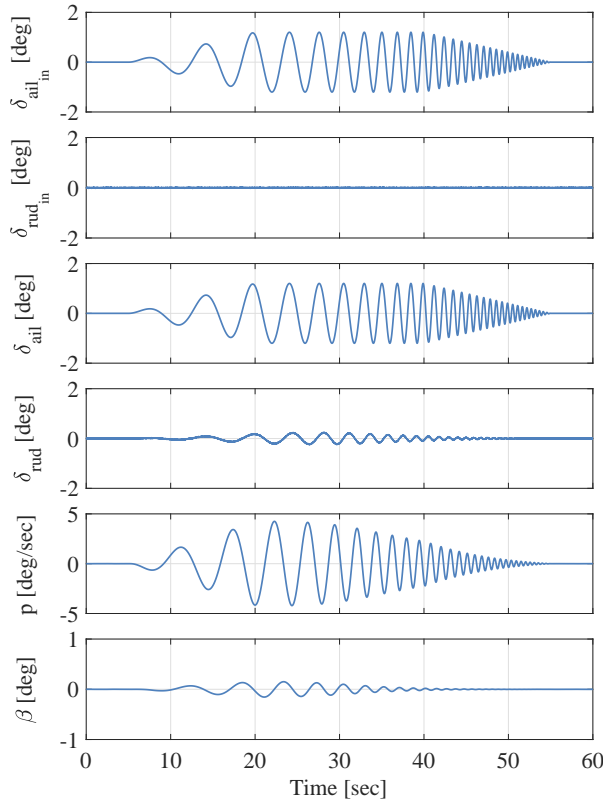


Figure 5. Closed-loop roll-axis frequency sweep time history (LJ-25 simulation example).

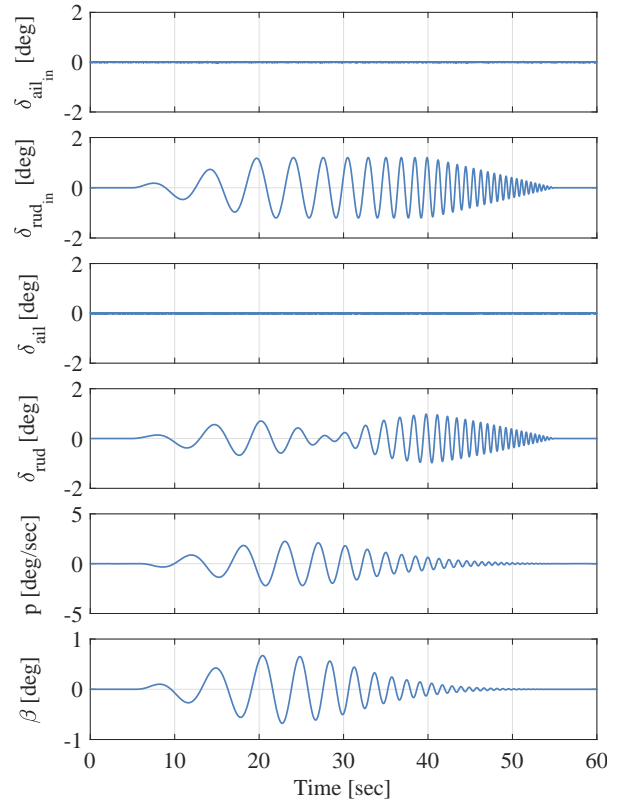


Figure 6. Closed-loop yaw-axis frequency sweep time history (LJ-25 simulation example).

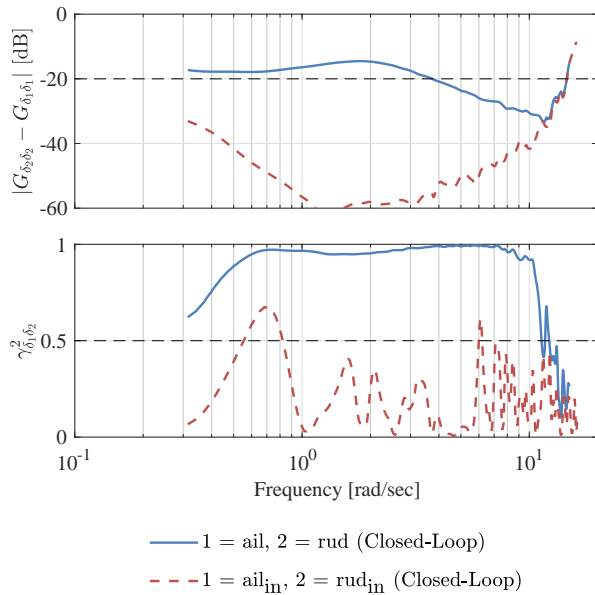


Figure 7. Closed-loop roll-axis frequency sweep cross-control correlation for aerosurface and actuator commands (LJ-25 simulation example).

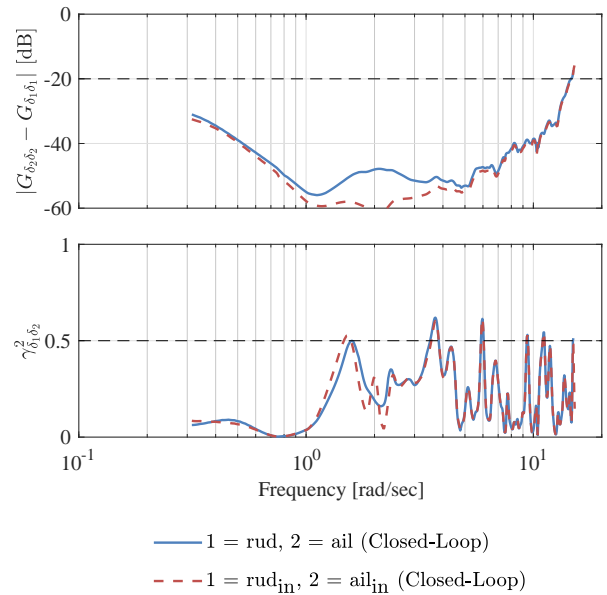


Figure 8. Closed-loop yaw-axis frequency sweep cross-control correlation for aerosurface and actuator commands (LJ-25 simulation example).

Fig. 8. In this case, since there is no feedback to the ailerons, both the bare-airframe inputs (primary input δ_{rud} and secondary input δ_{ail}) and the actuator command inputs (primary input $\delta_{rud,in}$ and secondary input $\delta_{ail,in}$) are not highly correlated (i.e., meet the guidelines in Eqs. 3 and 4). Therefore, we expect that processing the yaw-axis frequency sweep data using the MISO Direct Method will produce accurate frequency responses to rudder inputs.

2. Orthogonal Multisine Inputs

In addition to the frequency sweeps input at the actuator commands one at a time presented above, a simultaneous excitation of both actuator commands was performed using orthogonal multisine inputs.² Orthogonal multisine inputs have commonly been used to de-correlate bare-airframe inputs and perform system identification of multi-input systems using one time history record.² The orthogonal phase-optimized multisine signals input directly into the aileron and rudder actuator commands ($\delta_{ail,in}$, $\delta_{rud,in}$) in this example are given by:

$$\begin{aligned}\delta_{ail,in} &= \sum_{i_{ail}} a_{i_{ail}} \cos\left(\frac{2\pi i_{ail}}{T}t + \phi_{i_{ail}}\right), \quad i_{ail} = 1, 3, \dots, 39 \\ \delta_{rud,in} &= \sum_{i_{rud}} a_{i_{rud}} \cos\left(\frac{2\pi i_{rud}}{T}t + \phi_{i_{rud}}\right), \quad i_{rud} = 2, 4, \dots, 40\end{aligned}\quad (14)$$

where, $i_{ail} \neq i_{rud}$ ensures that the inputs are orthogonal.

Figure 9 shows the 40 excitation frequencies $\omega_i = 2\pi i/T$ (20 per input) used in each input and their corresponding magnitudes a_i . The phase lags ϕ_i were optimized to minimize the relative peak factor of the input signals.² Then, the magnitudes of each excitation frequency a_i were scaled to produce input magnitudes similar to the frequency sweeps presented above (± 1.2 deg). In addition, the same record length $T = 60$ sec was used for the multisine input as for the frequency sweeps, although here, the 5 sec of trim data at the beginning and end of the maneuver were not included, thus fully utilizing the $T = 60$ sec record length. In addition, since neither reference input ($\delta_{ail,in}$, $\delta_{rud,in}$) was exactly 0 in this case, no noise was added to the inputs.

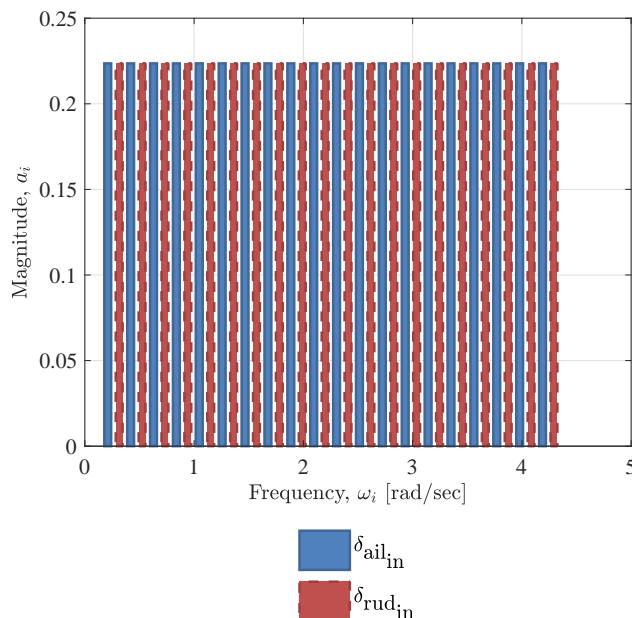


Figure 9. Multisine excitation frequencies for actuator command signals.

Figure 10 shows time histories of the aileron and rudder actuator command inputs ($\delta_{A,in} = [\delta_{ail,in} \ \delta_{rud,in}]^T$), bare-airframe aileron and rudder inputs ($\delta_A = [\delta_{ail} \ \delta_{rud}]^T$), and aircraft outputs ($\mathbf{y} = [p \ \beta]^T$) for the multisine signal.

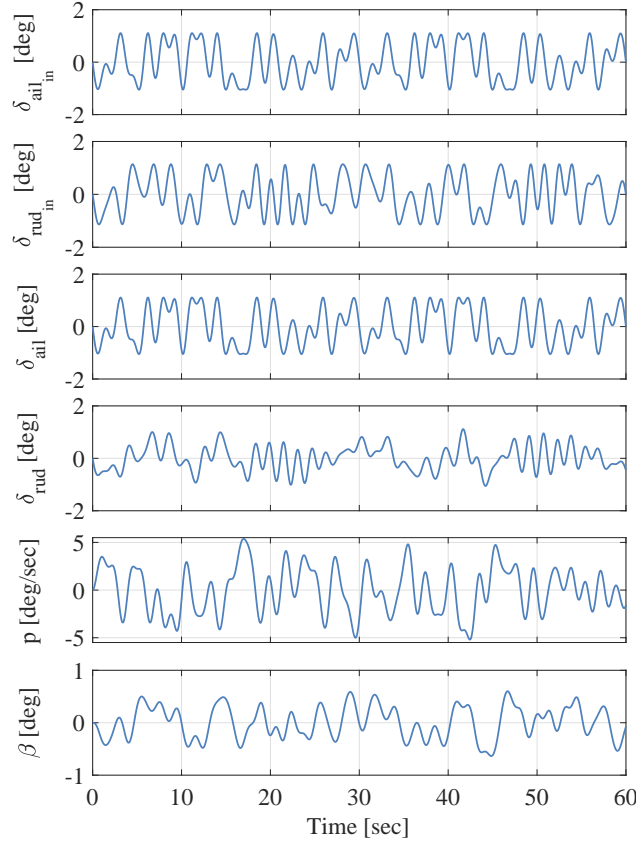


Figure 10. Closed-loop simultaneous roll- and yaw-axis phase-optimized orthogonal multisines time histories (LJ-25 simulation example).

A discrete finite Fourier transform evaluated only at the excitation frequencies was used to extract frequency responses from the multisine data.¹³ For example, the roll rate p responses are given by:

$$\begin{aligned} \frac{p}{\delta_{ail}}(j\omega_{i_{ail}}) &= \frac{\sum_{k=0}^{N-1} p(t_k)[\cos(\omega_{i_{ail}} t_k) - j \sin(\omega_{i_{ail}} t_k)]\Delta t}{\sum_{k=0}^{N-1} \delta_{ail}(t_k)[\cos(\omega_{i_{ail}} t_k) - j \sin(\omega_{i_{ail}} t_k)]\Delta t} \\ \frac{p}{\delta_{rud}}(j\omega_{i_{rud}}) &= \frac{\sum_{k=0}^{N-1} p(t_k)[\cos(\omega_{i_{rud}} t_k) - j \sin(\omega_{i_{rud}} t_k)]\Delta t}{\sum_{k=0}^{N-1} \delta_{rud}(t_k)[\cos(\omega_{i_{rud}} t_k) - j \sin(\omega_{i_{rud}} t_k)]\Delta t} \end{aligned} \quad (15)$$

where Δt is the sampling time and N is the number of data samples in the time history.

Although the multisine input signals used (δ_{ail_in} , δ_{rud_in}) are uncorrelated by design, the presence of feedback and bare-airframe coupling *results in correlation of the actual control surface deflections* (δ_{ail} , δ_{rud}). Figure 11 shows the magnitude of each excitation frequency in the bare-airframe inputs. As expected, only those excitation frequencies used in the aileron command input δ_{ail_in} are present in the aileron deflection δ_{ail} (Fig. 11, top subplot), since there is no feedback to the ailerons. In contrast, excitation frequencies used in both the aileron command input δ_{ail_in} and rudder command input δ_{rud_in} are present in the rudder deflection δ_{rud} (Fig. 11, bottom subplot). The presence of aileron command excitation frequencies in the rudder deflection is due to both inherent bare-airframe lateral/directional coupling (i.e., $\beta/\delta_{ail} \neq 0$) and presence of a yaw damper. A quantitative correlation analysis between the aileron and rudder deflections was done using correlation coefficients, given in Table 2. This correlation level is well below the 0.9 correlation level

typically used as an upper limit for allowable correlation of explanatory variables,² incorrectly suggesting that frequency responses extracted from the data using the Orthogonal DFT Method should match the bare-airframe for both aileron and rudder inputs.

Table 2. Pairwise correlation matrix for control surface deflections

| | δ_{ail} | δ_{rud} |
|-----------------------|-----------------------|-----------------------|
| δ_{ail} | 1 | 0.0319 |
| δ_{rud} | — | 1 |

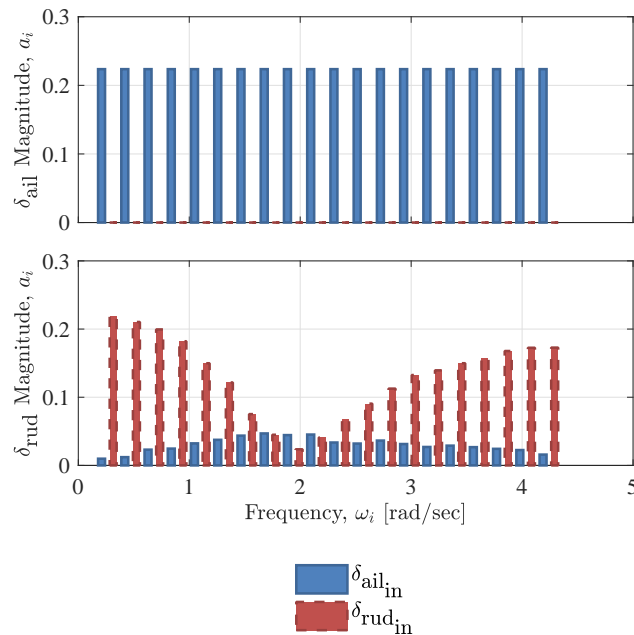


Figure 11. Multisine excitation frequencies in aerosurface deflections (LJ-25 simulation example).

3. Results

Figures 12 through 15 show the bare-airframe frequency responses of:

1. The known truth model,
2. Identified from the frequency sweep data using the SISO Direct Method,
3. Identified from the frequency sweep data using the JIO Method, and
4. Identified from the multisine data using the Orthogonal DFT Method.

The results of the different methods are compared using a standard and useful frequency-domain accuracy metric, the mismatch cost function J ,¹ which is the weighted sum of squared magnitude (dB) and phase (deg) errors between the identified response and true response. The mismatch costs for the SISO Direct and JIO Methods are calculated over the frequency range of $\omega = 0.3 - 10$ rad/sec. For the Orthogonal DFT Method, the mismatch costs are calculated at the 20 discrete frequency points. The cost for each response is shown in the legends of Figs. 12 through 15, as well as summarized in Table 3.

As expected, the responses to aileron input, p/δ_{ail} (Fig. 12) and $\beta/\delta_{\text{ail}}$ (Fig. 13), identified using the SISO Direct Method, where rudder inputs are ignored, are incorrect and have large mismatch costs: $J_{\text{SISO}_{p/\delta_{\text{ail}}}} = 43.38$ and $J_{\text{SISO}_{\beta/\delta_{\text{ail}}}} = 1096.14$. The frequency responses have an over-damped Dutch roll mode, due to the suppression of the Dutch roll oscillations by the yaw damper, which is not accounted for in the SISO Direct Method. Essentially, the SISO Direct Method identified the responses to aileron with the yaw-damper loop closed, instead of for the bare-airframe. Recall that the MISO Direct Method could not be used here,

because the secondary input was highly correlated to the primary input rendering the matrix $\mathbf{G}_{\delta_A \delta_A}$ in Eq. 2 nearly singular and therefore non-invertible.

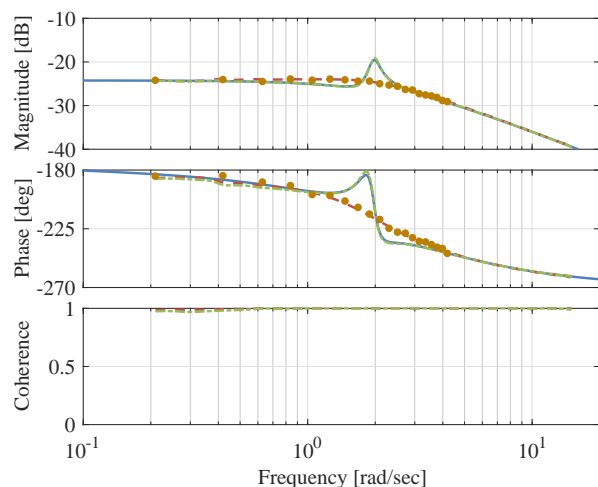
The responses to aileron input identified using the JIO Method agree with the bare-airframe model, retaining the correct peaking of the Dutch roll mode in the frequency responses and having significantly lower mismatch costs: $J_{\text{JIO } p/\delta_{\text{ail}}} = 0.88$ and $J_{\text{JIO } \beta/\delta_{\text{ail}}} = 3.23$.

The Orthogonal DFT Method gives results in close agreement to the SISO Direct Method (Figs. 12 and 13), in essence identifying the responses to aileron input with the yaw-damper loop closed, which is not reflective of the bare-airframe response. The Orthogonal DFT Method mismatch costs are slightly higher than the SISO Direct Method and significantly higher than the JIO Method: $J_{\text{DFT } p/\delta_{\text{ail}}} = 62.81$ and $J_{\text{DFT } \beta/\delta_{\text{ail}}} = 1691.82$. This is despite the low correlation coefficient between the aileron and rudder deflections (shown in Table 2).

Figures 14 and 15 show the roll rate p and sideslip β bare-airframe frequency responses to rudder input δ_{rud} . Here, as expected, all identification methods used produced similar responses that matched the bare-airframe model well. This is because there was no correlated input to the aileron during the rudder frequency sweep which is evidenced by the low cross-control correlation analysis shown in Fig. 8. There was also no correlated input to the aileron during the multisine input, which is evidenced by the lack of $\delta_{\text{rud, in}}$ excitation frequency content in the δ_{ail} response shown in Fig. 11. These results confirm the close agreement between the Orthogonal DFT and SISO Direct Methods for the same record length, with slightly better SISO Direct Method results, as shown previously in Ref. 14, due to higher spectral content of the frequency response input signal compared to the multisine signal.

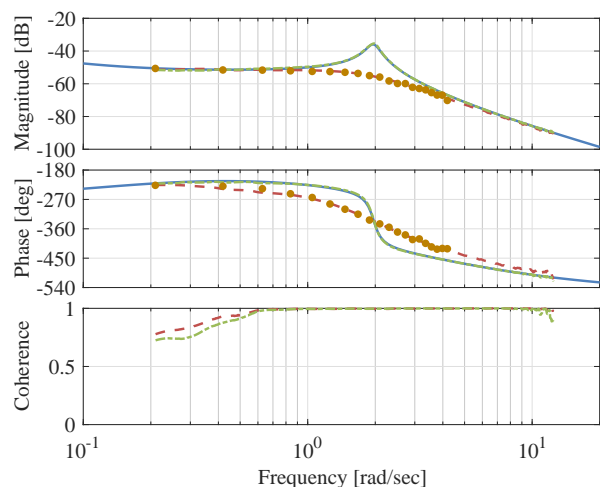
The results of Figs. 14 and 15 demonstrate that closed-loop identification of multi-input systems is not an issue when the inputs are truly de-correlated. When high input-correlation does exist (violating the guidelines in Eqs. 3 and 4), which can be generated with bare-airframe coupling and feedback or with crossfeeds, then identification using the MISO Direct Method cannot be used and the SISO Direct and Orthogonal DFT Methods will produce incorrect results, as shown in Figs. 12 and 13. For these cases of high input correlation, the JIO Method can produce correct results using the uncorrelated reference signals as the inputs.

Note that the JIO Method cannot be applied directly to frequency responses obtained from simultaneous multisine excitations using the Orthogonal DFT Method. This is because the columns of the $[\mathbf{y}/\mathbf{r}]$ and $[\delta_A/\mathbf{r}]$ matrices in Eq. 6 are each at different frequencies, by design of the orthogonal reference signals \mathbf{r} . Therefore, to apply the JIO Method to frequency responses obtained using the Orthogonal DFT Method, an additional step of interpolating all responses to a common frequency vector would be necessary before carrying out the calculation of Eq. 6.



— Bare-Airframe Model (Truth Data)
 - - - SISO Direct Method, Frequency Sweeps ($J = 43.38$)
 - · - JIO Method, Frequency Sweeps ($J = 0.88$)
 • Orthogonal DFT Method, Multisine ($J = 62.81$)

Figure 12. Roll rate to aileron (p/δ_{ail}) frequency response comparison (LJ-25 simulation example).



— Bare-Airframe Model (Truth Data)
 - - - SISO Direct Method, Frequency Sweeps ($J = 1096.14$)
 - · - JIO Method, Frequency Sweeps ($J = 3.23$)
 • Orthogonal DFT Method, Multisine ($J = 1691.82$)

Figure 13. Sideslip to aileron ($\beta/\delta_{\text{ail}}$) frequency response comparison (LJ-25 simulation example).

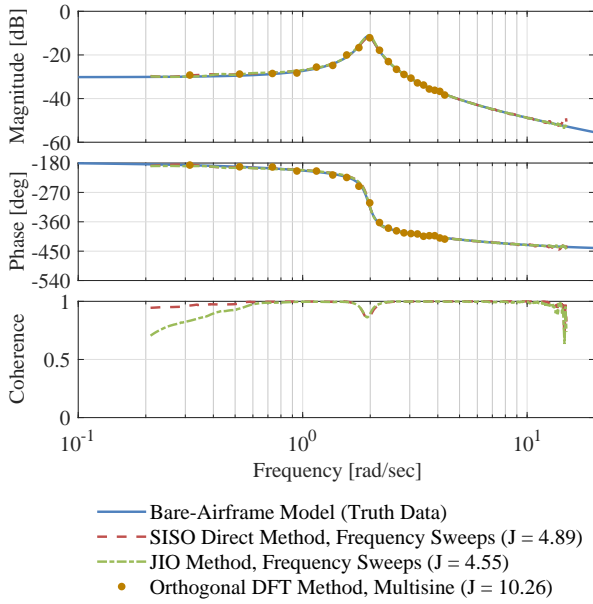


Figure 14. Roll rate to rudder (p/δ_{rud}) frequency response comparison (LJ-25 simulation example).

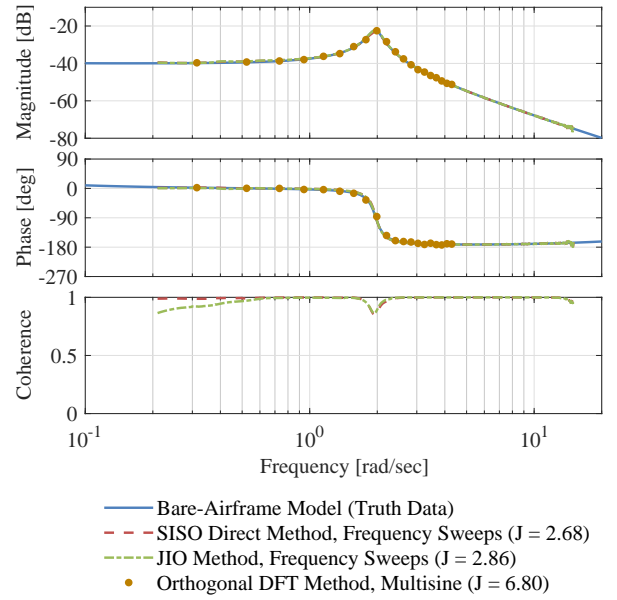


Figure 15. Sideslip to rudder (β/δ_{rud}) frequency response comparison (LJ-25 simulation example).

Table 3. Comparison of identification method mismatch costs J (LJ-25 simulation example)

| | SISO Direct | JIO | Orthogonal |
|----------------------|-------------|--------|------------|
| Response | Method | Method | DFT Method |
| p/δ_{ail} | 43.38 | 0.88 | 62.81 |
| β/δ_{ail} | 1096.14 | 3.23 | 1691.82 |
| p/δ_{rud} | 4.89 | 4.55 | 10.26 |
| β/δ_{rud} | 2.68 | 2.86 | 6.80 |

B. Compound Rotorcraft

In the second simulation example presented in this paper, the JIO method is applied to a notional high-speed compound rotorcraft with two coaxial main rotors and a pusher propeller. A rendering of the aircraft is shown in Fig. 16 and a detailed description of the flight dynamics of the aircraft model is provided in Ref. 15. This notional model is similar to the Sikorsky-Boeing SB>1 Defiant Joint Multi-Role (JMR) Technology Demonstrator (TD), and similar to one of the configurations being considered for the Future Vertical Lift (FVL) initiative.

With its two main rotors, pusher propeller, and vertical and horizontal tails, the configuration has multiple redundant controls. In total, the aircraft has 10 actuators: three actuator per main rotor (upper and lower), two pusher propeller actuators, one elevator actuator, and one rudder actuator. It is important to know the aircraft response to each individual actuator to be able to develop a control allocation scheme or for failure reconfiguration.

Closed-loop frequency sweeps were performed at 180 kts, Sea Level flight condition in simulation to extract the roll and pitch rate responses to each individual actuator. The model contained an explicit model following control system with pseudo-inverse control allocation. Since there are 10 bare-airframe actuators $\delta_A = [\delta_{A_1} \dots \delta_{A_{10}}]^T$, 10 reference inputs are needed for the identification $\mathbf{r} = [r_1 \dots r_{10}]^T$. In this example, the reference inputs \mathbf{r} are mixed to command the 10 actuators to produce symmetric and differential collective, longitudinal cyclic, and lateral cyclic, propeller collective, propeller lateral cyclic, elevator, and rudder inputs, through a mixing matrix \mathbf{M} given by:



Figure 16. High-speed compound rotorcraft rendering.

$$\underbrace{\begin{bmatrix} \delta_{A_{in1}} \\ \delta_{A_{in2}} \\ \delta_{A_{in3}} \\ \delta_{A_{in4}} \\ \delta_{A_{in5}} \\ \delta_{A_{in6}} \\ \delta_{A_{in7}} \\ \delta_{A_{in8}} \\ \delta_{A_{in9}} \\ \delta_{A_{in10}} \end{bmatrix}}_{\delta_A} = \underbrace{\begin{bmatrix} 0.866 & 0.5 & 1.0 & 1.0 & 0.866 & 0.5 & 0 & 0 & 0 & 0 \\ 0 & -1.0 & 1.0 & 1.0 & 0 & -1.0 & 0 & 0 & 0 & 0 \\ -0.866 & 0.5 & 1.0 & 1.0 & -0.866 & 0.5 & 0 & 0 & 0 & 0 \\ 0 & 1.0 & 1.0 & -1.0 & 0 & -1.0 & 0 & 0 & 0 & 0 \\ -0.866 & -0.5 & 1.0 & -1.0 & 0.866 & 0.5 & 0 & 0 & 0 & 0 \\ 0.866 & -0.5 & 1.0 & -1.0 & -0.866 & 0.5 & 0 & 0 & 0 & 0 \\ 0 & 0 & 0 & 0 & 0 & 0 & 1.0 & 0 & 0 & 0 \\ 0 & 0 & 0 & 0 & 0 & 0 & 0 & 1.0 & 0 & 0 \\ 0 & 0 & 0 & 0 & 0 & 0 & 0 & 0 & 1.0 & 0 \\ 0 & 0 & 0 & 0 & 0 & 0 & 0 & 0 & 0 & 1.0 \end{bmatrix}}_M \underbrace{\begin{bmatrix} r_1 \\ r_2 \\ r_3 \\ r_4 \\ r_5 \\ r_6 \\ r_7 \\ r_8 \\ r_9 \\ r_{10} \end{bmatrix}}_r \quad (16)$$

Table 4 lists the 10 reference inputs used and the 10 bare-airframe actuators. The mixed reference input $\delta_{A_{in}}$ is then summed into the actuator commands as shown in Fig. 2. Note that although the reference inputs are excited only one at a time, the mixing of the reference inputs and the control system fully correlate the bare-airframe inputs δ_A .

Table 4. Compound rotorcraft reference signals and actuators

| Reference Input | | Actuator | |
|-----------------|----------------------------------|-------------------|-------------------------------|
| Symbol | Name | Symbol | Name |
| r_1 | Symmetric lateral cyclic | δ_{A_1} | Upper rotor actuator 1 |
| r_2 | Symmetric longitudinal cyclic | δ_{A_2} | Upper rotor actuator 2 |
| r_3 | Symmetric collective | δ_{A_3} | Upper rotor actuator 3 |
| r_4 | Differential collective | δ_{A_4} | Lower rotor actuator 1 |
| r_5 | Differential lateral cyclic | δ_{A_5} | Lower rotor actuator 2 |
| r_6 | Differential longitudinal cyclic | δ_{A_6} | Lower rotor actuator 3 |
| r_7 | Propellor collective | δ_{A_7} | Propellor collective actuator |
| r_8 | Propellor lateral cyclic | δ_{A_8} | Propellor cyclic actuator |
| r_9 | Elevator | δ_{A_9} | Elevator actuator |
| r_{10} | Rudder | $\delta_{A_{10}}$ | Rudder actuator |

Ten closed-loop frequency sweeps are performed, exciting each reference signal r_i individually. Figures 17 and 18 show time histories of two of the 10 sweep maneuvers: symmetric lateral cyclic r_1 and symmetric longitudinal cyclic r_2 , respectively. The total sweep length used is $T = 120$ sec for each maneuver, including 5 sec of trim data at the beginning and end of the maneuver. The range of frequencies excited during the sweep is $\omega = 0.6 - 20$ rad/sec. For each maneuver, a sweep amplitude of ± 2.0 deg was used on the swept reference input (shown in Figs. 17 and 18), while ± 0.01 deg white noise was added to the nine other non-swept reference inputs (not shown in Figs. 17 and 18). Therefore, for each frequency sweep maneuver, the reference inputs \mathbf{r} are not correlated by design.

Figures 17 and 18 also show time histories for four of the 10 bare-airframe actuators: upper rotor actuator 1 δ_{A_1} , lower rotor actuator 1 δ_{A_4} , elevator actuator δ_{A_9} , and rudder actuator $\delta_{A_{10}}$. In addition, the roll rate p and pitch rate q time histories are shown.

During the symmetric lateral cyclic r_1 sweep (Fig. 17), the upper and lower rotor actuators δ_{A_1} and δ_{A_4} as well as the rudder actuator $\delta_{A_{10}}$ are fully correlated (as seen by the second, third, and fifth subplots in Fig. 17). Furthermore, as expected for this input, the aircraft is primarily excited in roll ($p \approx \pm 20$ deg/sec, sixth subplot in Fig. 17) with minor pitch excitations ($q \approx \pm 0.5$ deg/sec, seventh subplot in Fig. 17).

During the symmetric longitudinal cyclic r_2 sweep (Fig. 18), the upper and lower rotor actuators δ_{A_1} and δ_{A_4} as well as the elevator actuator δ_{A_9} and rudder actuator $\delta_{A_{10}}$ are fully correlated (as seen by the second through fifth subplots in Fig. 17). Furthermore, as expected for this input, the aircraft is primarily excited in pitch ($q \approx \pm 20$ deg/sec, seventh subplot in Fig. 17) with minor roll excitations ($p \approx \pm 0.5$ deg/sec, sixth subplot in Fig. 17).

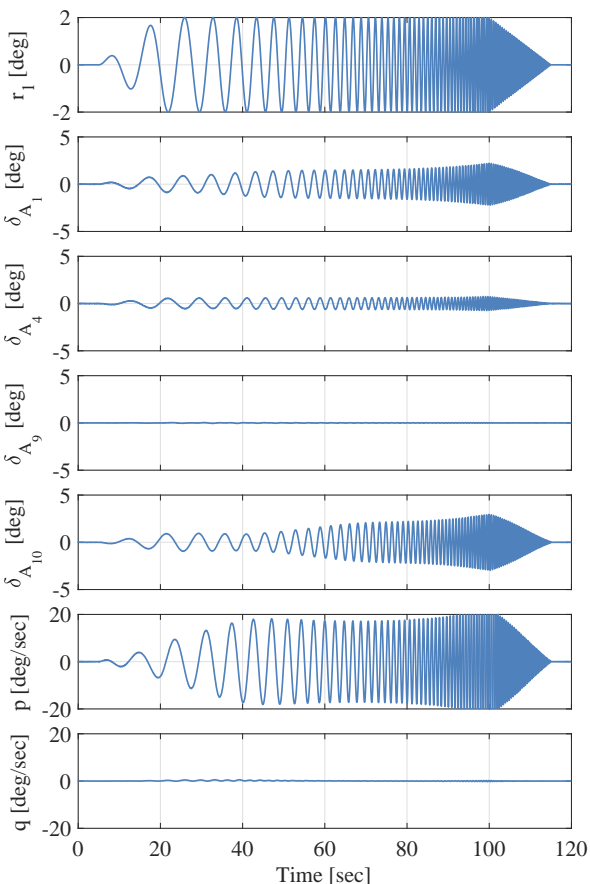


Figure 17. Closed-loop symmetric lateral cyclic r_1 sweep frequency sweep (Compound rotorcraft simulation example).

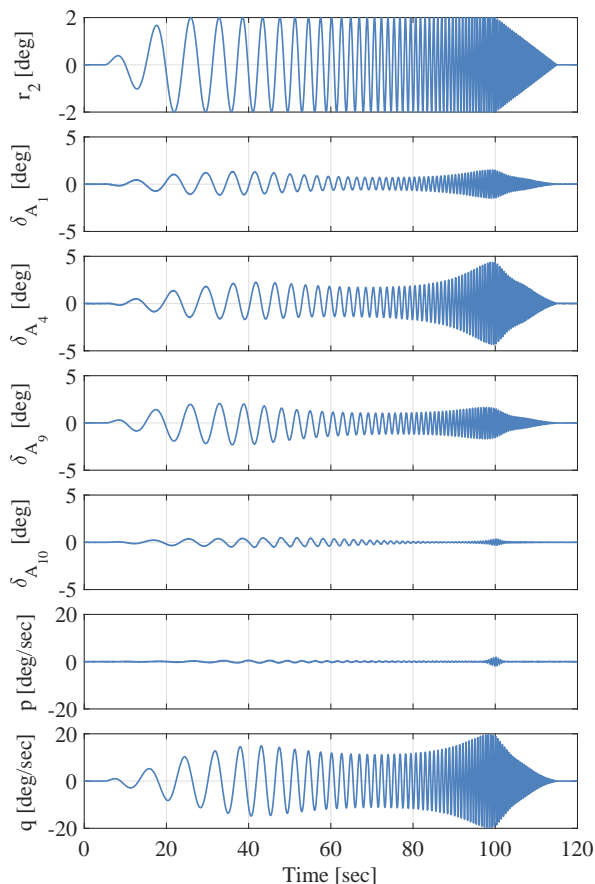


Figure 18. Closed-loop symmetric longitudinal cyclic r_2 sweep frequency sweep (Compound rotorcraft simulation example).

A quantitative cross-control correlation analysis was performed to confirm the bare-airframe input correlation for the symmetric lateral cyclic r_1 sweep seen qualitatively from the time histories in Fig. 17. Figure 19

shows the cross-control coherence, which is a correlation analysis in the frequency domain, for the symmetric lateral cyclic r_1 sweep between four of the 10 bare-airframe inputs (primary input δ_{A_1} and secondary inputs δ_{A_4} , δ_{A_9} , and $\delta_{A_{10}}$). The cross-control coherence (Fig. 19, bottom subplot) is $\gamma_{\delta_1 \delta_2}^2 \approx 1.0$ over a broad frequency range, violating the guideline in Eq. 3. For the elevator actuator δ_{A_9} , the secondary input magnitude is small and meets the guideline in Eq. 3 (Fig. 19, top subplot, dashed red line). Therefore, the elevator actuator input can be ignored in the analysis. However, since not all secondary inputs meet the guidelines of Eqs. 3 and 4, the SISO Direct Method *will produce incorrect results*.

Figure 20 shows the cross-control correlation analysis for the symmetric lateral cyclic r_1 sweep between four of the 10 reference inputs (primary input r_1 and secondary inputs r_4 , r_9 , and r_{10}). Here, the cross-control coherence and secondary input magnitudes are all low (meet the guidelines in Eqs. 3 and 4). Therefore, the MISO Direct Method can be applied to the data with the reference signals as the inputs. Then, the JIO Method is applied to post process the results and extract the bare-airframe frequency responses.

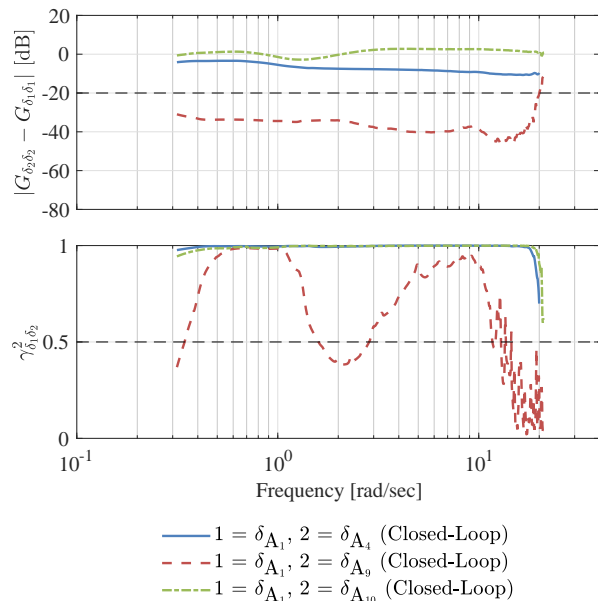


Figure 19. Closed-loop symmetric lateral cyclic frequency sweep cross-control correlation for actuator positions (Compound rotorcraft simulation example).

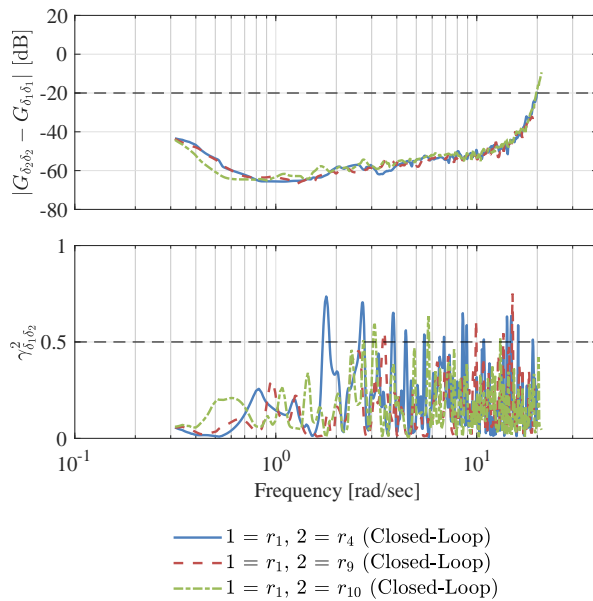


Figure 20. Closed-loop symmetric lateral cyclic frequency sweep cross-control correlation for reference signals (Compound rotorcraft simulation example).

A representative subset of the 20 identified frequency responses (p/δ_{A_i} and q/δ_{A_i} , $i = 1 \dots 10$) are presented here for brevity. Figures 21 through 24 show the roll rate p bare-airframe frequency responses to upper rotor actuator 1 input δ_{A_1} , lower rotor actuator 1 input δ_{A_4} , elevator actuator input δ_{A_9} , and rudder actuator input $\delta_{A_{10}}$ for the bare-airframe model (truth data) and as extracted from the closed-loop sweeps using the SISO Direct and JIO Method. Note that the SISO Direct Method results are shown for comparison when the secondary controls are ignored, since the cross-control correlation results in a breakdown of the MISO Direct Method. Mismatch costs J are given for the identified responses as compared to the known bare-airframe model.

For all responses, the results extracted using the JIO Method show excellent agreement with the bare-airframe model. This is even the case for the off-axis response of roll rate to elevator p/δ_{A_9} shown in Fig. 23. In contrast, the results extracted using the SISO Direct Method show very poor agreement, as expected due to the high cross-control correlation, even while having high coherence.

Figures 25 and 26 show the pitch rate q bare-airframe frequency responses to lower rotor actuator 1 input δ_{A_4} and elevator actuator input δ_{A_9} for the bare-airframe model (truth data) and as extracted from the closed-loop sweeps using the SISO Direct and JIO Method. As with the roll rate responses shown, the results extracted using the JIO Method show excellent agreement with the bare-airframe model, while the results extracted using the SISO Direct Method show very poor agreement.

The remaining results (not presented) show similar levels of agreements between the frequency responses identified using the JIO Method and the known bare-airframe model. These results validate using the JIO

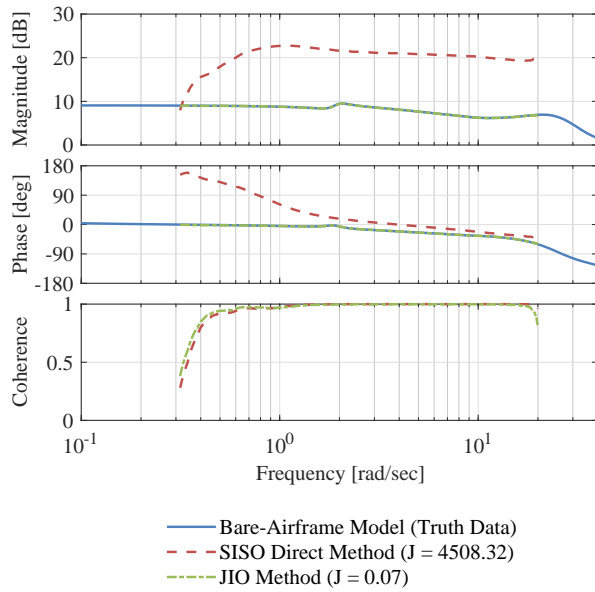


Figure 21. Roll rate to upper rotor actuator 1 (p/δ_{A_1}) frequency response comparison (Compound rotorcraft simulation example).

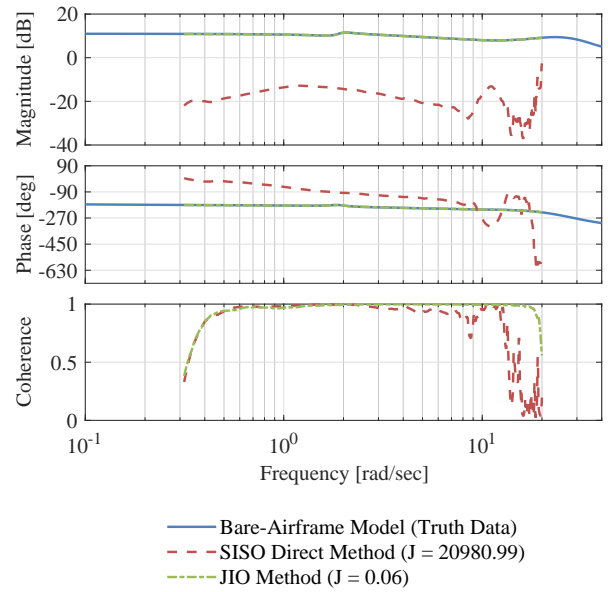


Figure 22. Roll rate to lower rotor actuator 1 (p/δ_{A_4}) frequency response comparison (Compound rotorcraft simulation example).

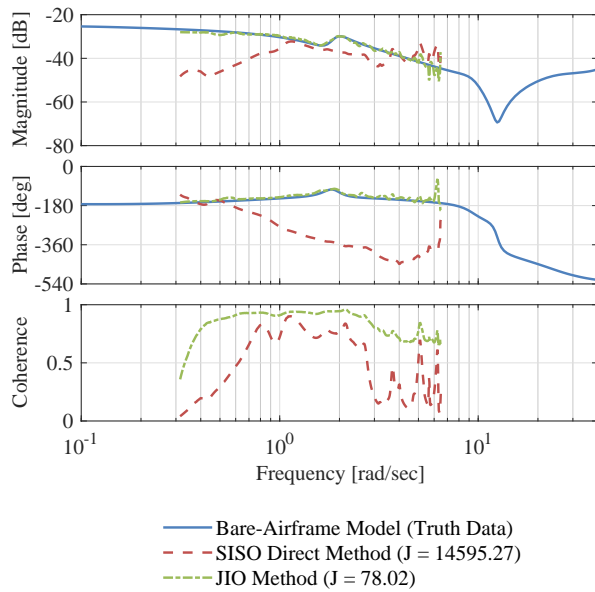


Figure 23. Roll rate to elevator (p/δ_{A_9}) frequency response comparison (Compound rotorcraft simulation example).

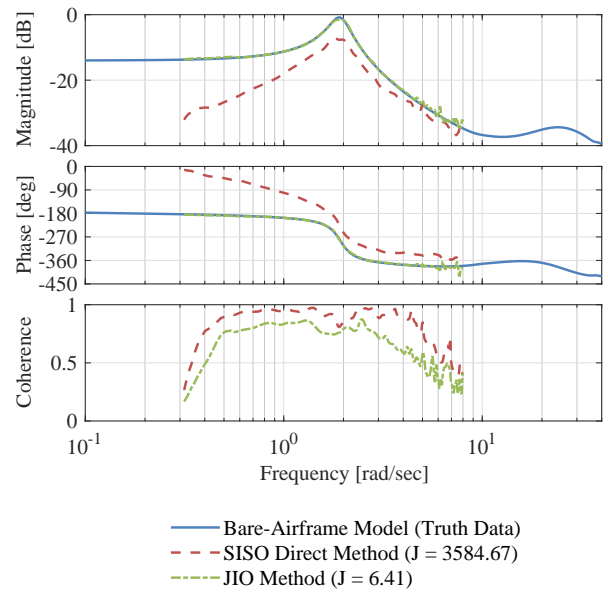


Figure 24. Roll rate to rudder ($p/\delta_{A_{10}}$) frequency response comparison (Compound rotorcraft simulation example).

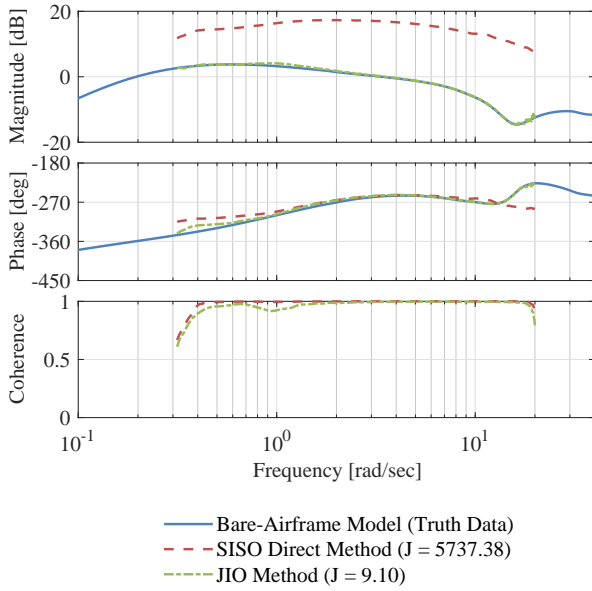


Figure 25. Pitch rate to lower rotor actuator 1 (q/δ_{A_4}) frequency response comparison (Compound rotorcraft simulation example).

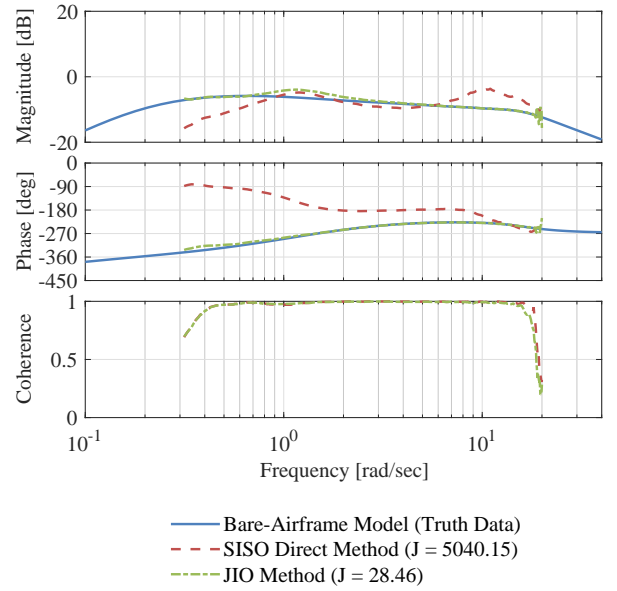


Figure 26. Pitch rate to elevator (q/δ_{A_9}) frequency response comparison (Compound rotorcraft simulation example).

Method when the reference inputs are mixed before they are summed to the individual actuator commands, as in Fig. 2.

IV. Flight-Test Examples

To demonstrate that the JIO Method works on real flight-test data where noise and turbulence are present, two flight-test examples are presented in this section. The first flight-test example is based on identification of a Learjet LJ-25D lateral/directional dynamics from closed-loop flight data. The second flight-test example is based on identification of an octocopter UAV frequency responses to each individual motor.

A. Learjet LJ-25D

This example is based on identification of the Calspan Variable Stability System (VSS) Learjet LJ-25D (Fig. 3) lateral/directional dynamics from closed-loop flight-test data. The control system used during the closed-loop frequency sweeps, described in detail in Refs. 16 and 17, contains crossfeeds between the lateral and directional axes in both the feed-forward (\mathbf{F} in Fig. 1) and feedback (\mathbf{H} in Fig. 1) paths, thus fully correlating the bare-airframe aerosurface inputs aileron δ_{ail} and rudder δ_{rud} . Since δ_A is fully correlated, the MISO Direct Method cannot be applied using δ_A as the input. Therefore, bare-airframe frequency responses are extracted from closed-loop flight data using the JIO Method for piloted frequency sweeps, with δ_S in Fig. 1 used as the reference input. The resulting JIO frequency responses are compared to those extracted from open-loop piloted frequency sweeps using the MISO Direct Method where the bare-airframe inputs were not correlated (i.e., the truth data). In addition, the JIO frequency responses are compared to those extracted from the closed-loop data with δ_A as the input processed using the SISO Direct Method (which will produce incorrect results in this case).

Figure 27 shows time histories of the pilot lateral stick and pedal inputs ($\delta_S = [\delta_{lat} \delta_{ped}]^T$), bare-airframe aileron and rudder inputs ($\delta_A = [\delta_{ail} \delta_{rud}]^T$), and aircraft outputs ($\mathbf{y} = [p \beta]^T$) for both the open- and closed-loop roll-axis frequency sweeps. During both open- and closed-loop sweeps, there is no input on the pedals δ_{ped} (Fig. 27, second subplot), and therefore the pilot inputs δ_S are not correlated. For the open-loop sweeps, the rudder deflections δ_{rud} (secondary input) during the maneuver are significantly smaller than and not correlated with the aileron deflections (primary input) (Fig. 27, fourth subplot, solid blue line). However, for the closed-loop sweeps, the control system produced rudder inputs that are highly correlated with the

aileron inputs (violates the guideline in Eq. 3) and have a large magnitude (violates the guideline in Eq. 4) (Fig. 27, fourth subplot, dashed red line). In addition, during the closed-loop sweeps, the control system suppressed the Dutch roll motion of the aircraft, as evidenced by the significantly smaller sideslip response at around $t = 90$ sec in Fig. 27.

Figure 28 shows time histories for both the open- and closed-loop yaw-axis frequency sweeps. As with the roll-axis sweeps above, the pilot inputs δ_S are not correlated for both the open- and closed-loop sweeps. For the open-loop sweeps, the aileron deflections δ_{ail} (secondary input) are not correlated with the rudder deflections δ_{rud} (primary input). However, for the closed-loop sweeps, the control system produced large aileron inputs that are highly correlated with the rudder inputs (violating the guideline in Eqs. 3 and 4) (Fig. 28, third subplot, dashed red line). In addition, during the closed-loop sweeps, the control system almost entirely suppressed the roll motion of the aircraft, as evidenced by the significantly smaller roll rate response throughout the maneuver in Fig. 28.

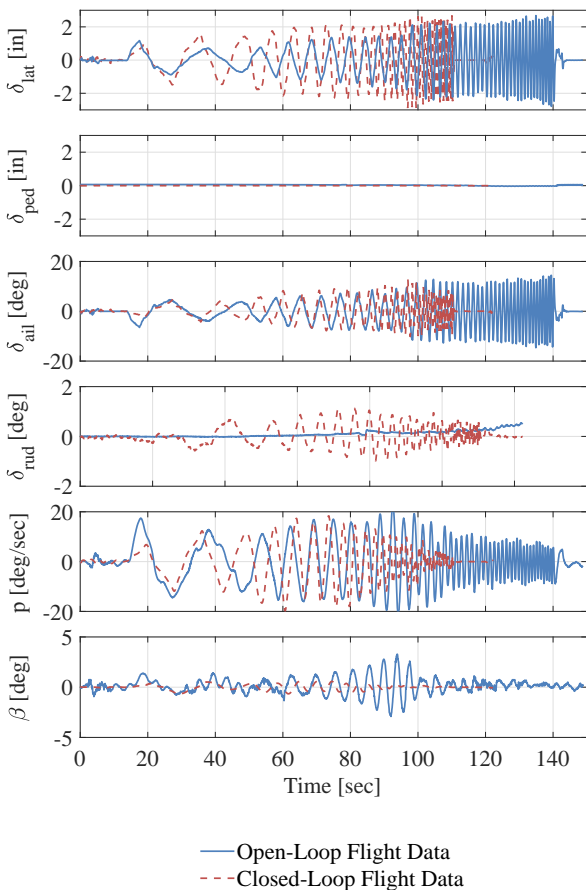


Figure 27. Open-loop and closed-loop roll-axis piloted frequency sweeps (LJ-25 flight-test example).

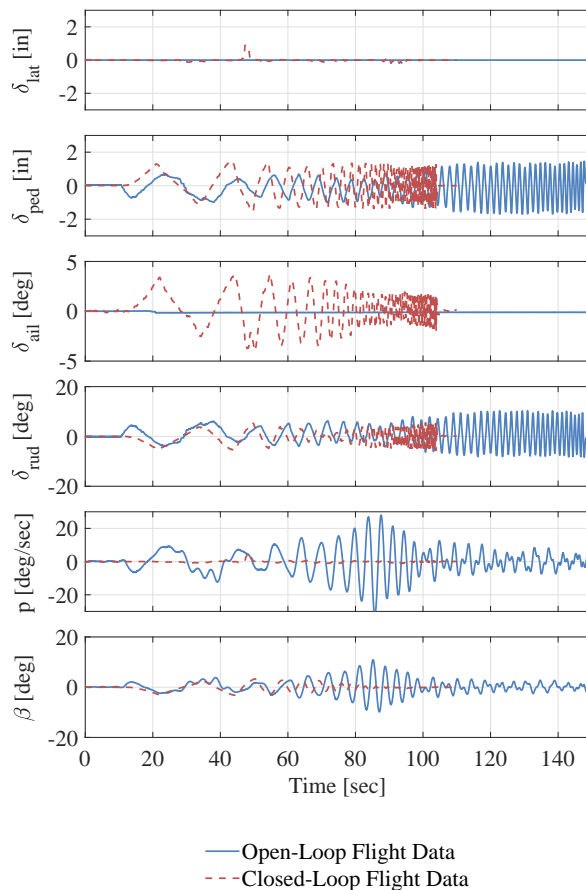


Figure 28. Open-loop and closed-loop yaw-axis piloted frequency sweeps (LJ-25 flight-test example).

A quantitative cross-control correlation analysis was performed to confirm the bare-airframe input correlation for the open- and closed-loop frequency sweeps seen qualitatively from the time histories in Figs. 27 and 28. Figure 29 shows the cross-control correlation analysis for both the open- and closed-loop roll-axis sweep data, while Fig. 30 shows the cross-control correlation analysis for both the open- and closed-loop yaw-axis sweep data. For the open-loop sweeps, the cross-control coherence between the bare-airframe inputs δ_{ail} , δ_{rud} for both the roll and yaw sweeps are $\gamma_{\delta_{ail}\delta_{rud}}^2, \gamma_{\delta_{rud}\delta_{ail}}^2 < 0.5$ (Figs. 29 and 30, bottom plot, solid blue line), indicating very little correlation between the primary and secondary inputs, and that the MISO Direct Method solution of Eq. 2 can be used. For the closed-loop sweeps, there is near-total correlation between the bare-airframe inputs for both the roll and yaw sweeps: $\gamma_{\delta_{ail}\delta_{rud}}^2, \gamma_{\delta_{rud}\delta_{ail}}^2 \approx 1.0$ across a large frequency

range (Figs. 29 and 30, bottom plot, dashed red line). Therefore, traditional conditioning of the responses using the MISO Direct Method identification technique cannot be used in this case. One approach is to ignore the secondary input and process the data using the SISO Direct Method, however, this will produce the wrong results since the secondary input magnitude is large compared to the primary input magnitude (Figs. 29 and 30, top plot, dashed red line).

However, if the pilot stick inputs δ_{lat} , δ_{ped} are used instead of the bare-airframe inputs for the closed-loop sweeps, the cross-control coherence values are all low (Figs. 29 and 30, bottom plot, dash-dot green line). Therefore, the MISO Direct Method is applied to the closed-loop data using the pilot stick as the input ($\mathbf{r} = \boldsymbol{\delta}_S = [\delta_{\text{lat}} \ \delta_{\text{ped}}]^T$) to extract $[\mathbf{y}/\boldsymbol{\delta}_S]$ and $[\boldsymbol{\delta}_A/\boldsymbol{\delta}_S]$. Then, the JIO Method is applied to extract the bare-airframe frequency responses as in Eq. 7.

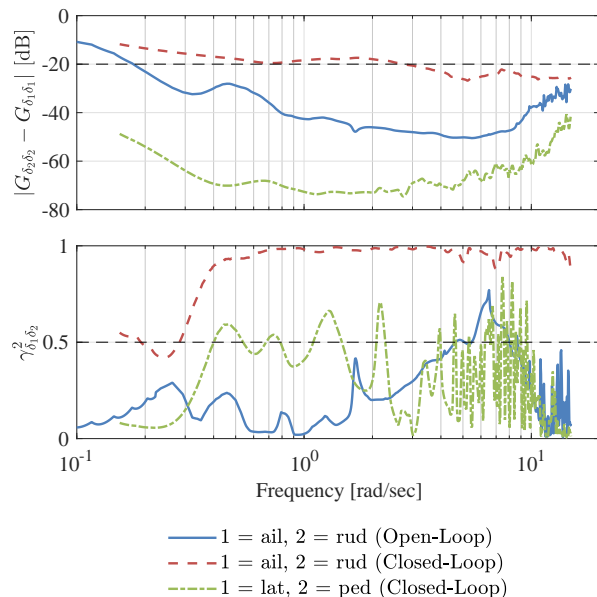


Figure 29. Open-loop and closed-loop roll-axis frequency sweep cross-control correlation for aerosurface and pilot inputs (LJ-25 flight-test example).

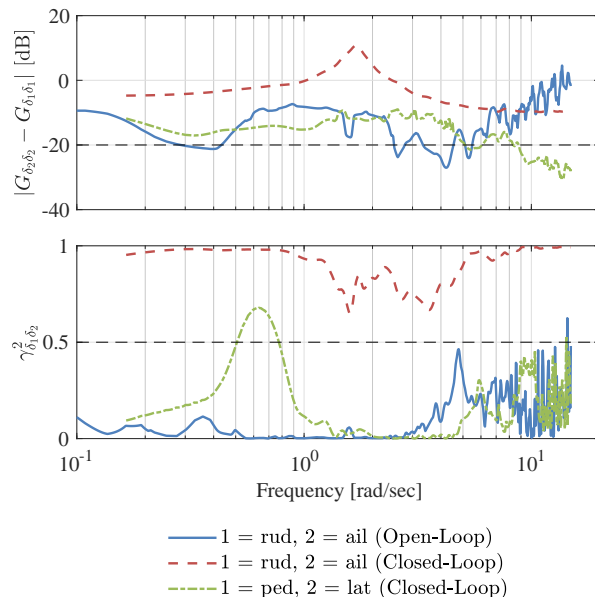


Figure 30. Open-loop and closed-loop yaw-axis frequency sweep cross-control correlation for aerosurface and pilot inputs (LJ-25 flight-test example).

Figures 31 and 32 show the roll rate p and sideslip β bare-airframe frequency responses to aileron input δ_{ail} as extracted from the open-loop sweeps using the MISO Direct Method (considered here as the truth data for the purposes of comparing methods). The figures also show the bare-airframe frequency responses as extracted from the closed-loop sweeps using the SISO Direct Method and JIO Method. Mismatch costs J are given for the responses identified from closed-loop data using the SISO Direct and JIO Methods as compared to the responses identified from open-loop data using the MISO Direct Method.

Both responses p/δ_{ail} , $\beta/\delta_{\text{ail}}$ determined from closed-loop data using the SISO Direct Method have an over-damped Dutch roll mode, due to the suppression of the Dutch roll oscillations by the control system. However, the JIO Method agrees with the open-loop data processed using the MISO Direct Method, retaining the correct peaking of the Dutch roll mode in the frequency responses, even though the yaw control system was suppressing this motion (Fig. 27, bottom plot). The better agreement of the JIO Method frequency responses with the truth data is also seen in their lower mismatch costs J as compared to the responses identified using the SISO Direct Method, especially for the (off-axis) sideslip response.

Figures 33 and 34 show the roll rate p and sideslip β bare-airframe frequency responses to rudder input δ_{rud} as extracted from the open-loop sweeps (MISO Direct Method) and from the closed-loop sweeps (SISO Direct Method and JIO Method). The roll rate response to rudder p/δ_{rud} was completely suppressed by the control system (Fig. 28, fifth subplot, dashed red line), and so the resulting frequency response extracted from the closed-loop sweeps using the SISO Direct Method has very low coherence and a large mismatch cost (Fig. 33). However, the p/δ_{rud} response is identified correctly using the JIO Method, as seen by the good agreement with the open-loop MISO Direct Method results (truth data), and has high coherence across a broad frequency range. The sideslip response to rudder $\beta/\delta_{\text{rud}}$ identified from the closed-loop data using the

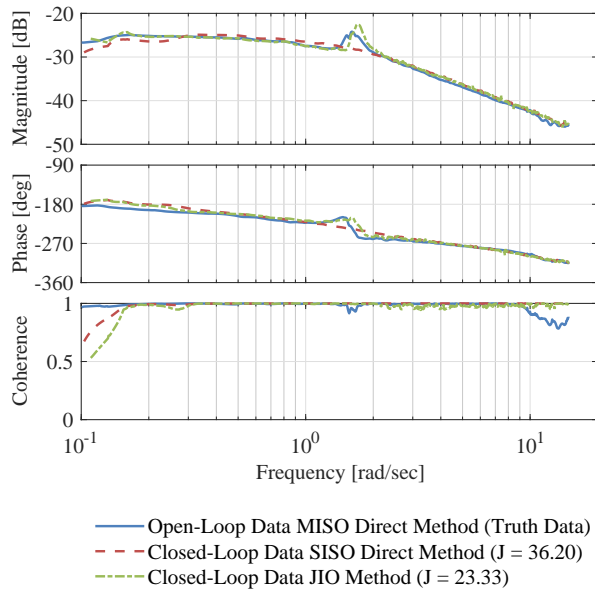


Figure 31. Roll rate to aileron (p/δ_{ail}) frequency response comparison (LJ-25 flight-test example).

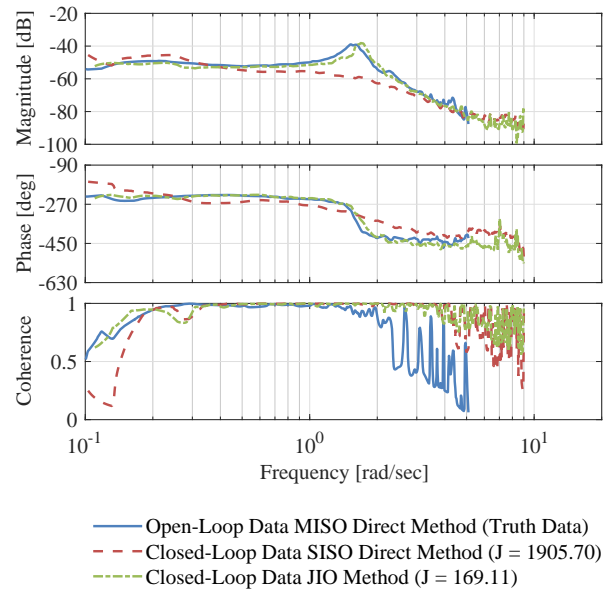


Figure 32. Sideslip to aileron (β/δ_{ail}) frequency response comparison (LJ-25 flight-test example).

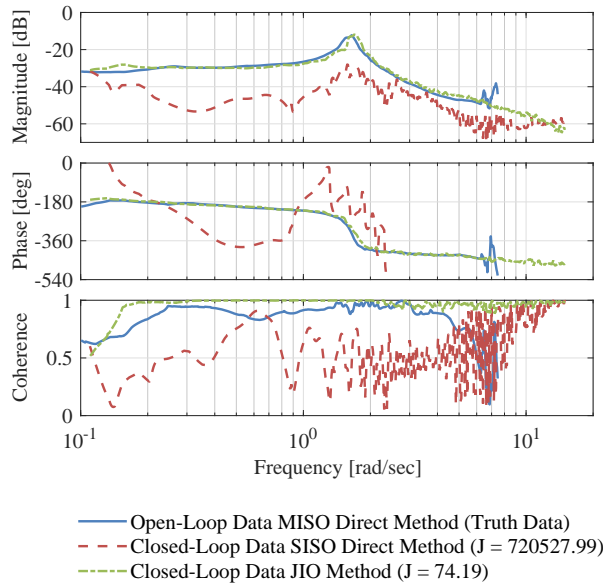


Figure 33. Roll rate to rudder (p/δ_{rud}) frequency response comparison (LJ-25 flight-test example).

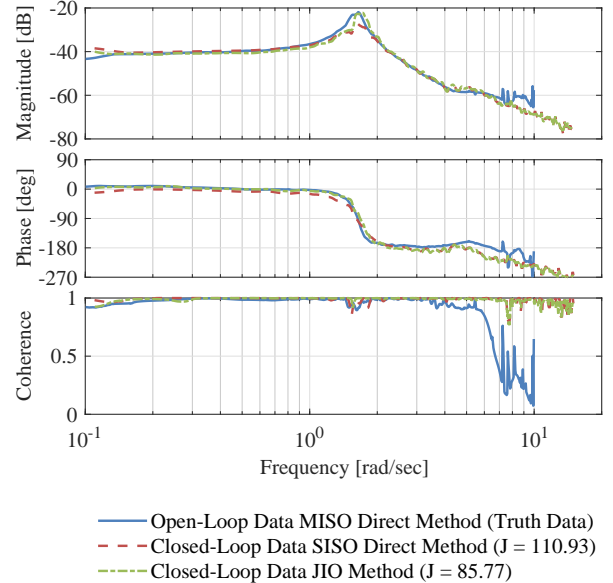


Figure 34. Sideslip to rudder (β/δ_{rud}) frequency response comparison (LJ-25 flight-test example).

SISO Direct Method has a distortion in the magnitude curve at the Dutch roll mode frequency $\omega_{dr} = 1.6$ rad/sec (Fig. 34). The β/δ_{rud} frequency response identified from the closed-loop data using the JIO Method matches the response identified from the open-loop data better and with a lower mismatch cost.

For all four responses shown, the frequency responses extracted from the closed-loop sweeps using the JIO Method match the open-loop frequency responses nearly perfectly. In contrast, the frequency responses extracted from the closed-loop data using the SISO Direct Method exhibited an over-predicted Dutch roll damping and wrong off-axis response characteristics, as expected.

B. Octocopter UAV

In the second flight-test example presented in this paper, the JIO method is applied to identify the dynamics of an octocopter UAV [shown in Fig. 35(a)]. This octocopter is a version of the vehicle presented in Ref. 18, originally built for studying package delivery but modified here with no cargo bay. The responses of the octocopter to the eight individual motors is needed to validate reconfigurable models (as done in Ref. 19) and to design control systems that included failure reconfiguration. The numbering convention, grouping, and direction of rotation of the eight motors is shown in the diagram in Fig. 35(b).

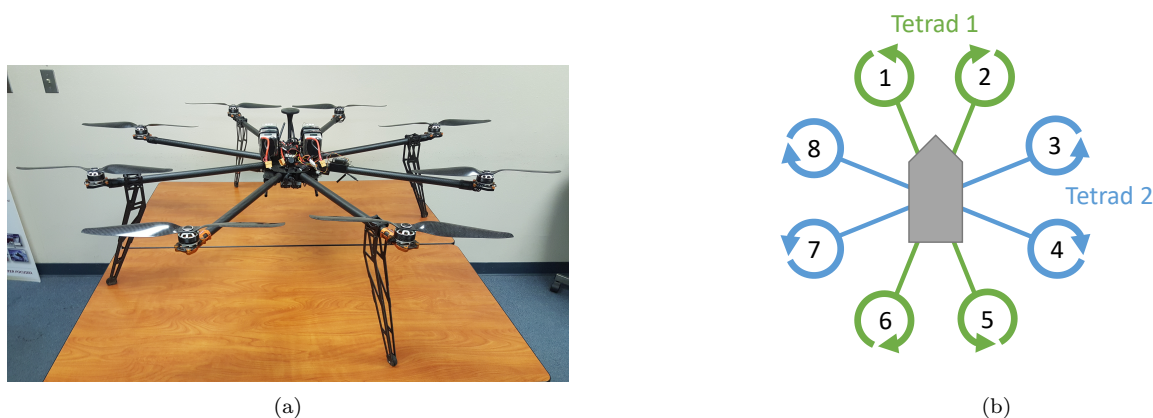


Figure 35. Octocopter UAV (a) picture and (b) motor numbering and rotation convention.

A closed-loop flight test was performed in which eight closed-loop frequency sweeps were performed, summing reference inputs directly into the motor commands generated by the flight control system. Similar to the compound rotorcraft example presented in Sec. III.B, the reference frequency sweep inputs were mixed before being summed into the motor commands, as shown in Fig. 2. The mixing matrix M , shown in Eq. 17, was selected to break the eight motors into a pair of tetrads (i.e., two groups of four), the first consisting of the front and back two motors [motors 1, 2, 5, and 6 in Fig. 35(b)] and the second consisting of the left and right two motors [motors 3, 4, 7, and 8 in Fig. 35(b)]. Each tetrad was then actuated to produce heave (r_1 and r_5), pitch (r_2 and r_6), roll (r_3 and r_7), and yaw (r_4 and r_8) responses. The eight reference inputs used are listed in Table 5.

$$\underbrace{\begin{bmatrix} \delta_{A_{in1}} \\ \delta_{A_{in2}} \\ \delta_{A_{in3}} \\ \delta_{A_{in4}} \\ \delta_{A_{in5}} \\ \delta_{A_{in6}} \\ \delta_{A_{in7}} \\ \delta_{A_{in8}} \end{bmatrix}}_{\delta_A} = \underbrace{\begin{bmatrix} 1 & 1 & 1 & 1 & 0 & 0 & 0 & 0 \\ 1 & 1 & -1 & -1 & 0 & 0 & 0 & 0 \\ 0 & 0 & 0 & 0 & 1 & 1 & -1 & 1 \\ 0 & 0 & 0 & 0 & 1 & -1 & -1 & -1 \\ 1 & -1 & -1 & 1 & 0 & 0 & 0 & 0 \\ 1 & -1 & 1 & -1 & 0 & 0 & 0 & 0 \\ 0 & 0 & 0 & 0 & 1 & -1 & 1 & 1 \\ 0 & 0 & 0 & 0 & 1 & 1 & 1 & -1 \end{bmatrix}}_M \underbrace{\begin{bmatrix} r_1 \\ r_2 \\ r_3 \\ r_4 \\ r_5 \\ r_6 \\ r_7 \\ r_8 \end{bmatrix}}_r \quad (17)$$

Table 5. Octocopter reference inputs

| Symbol | Name |
|--------|----------------|
| r_1 | Tetrad 1 heave |
| r_2 | Tetrad 1 pitch |
| r_3 | Tetrad 1 roll |
| r_4 | Tetrad 1 yaw |
| r_5 | Tetrad 2 heave |
| r_6 | Tetrad 2 pitch |
| r_7 | Tetrad 2 roll |
| r_8 | Tetrad 2 yaw |

Figures 36 and 37 show time histories of two of the eight sweep maneuvers: Tetrad 1 roll r_3 sweep and Tetrad 2 pitch r_6 sweep, respectively. The total sweep length used is $T = 70$ sec for each maneuver, including 5 sec of trim data at the beginning and end of the maneuver. The range of frequencies excited during the sweep is $\omega = 0.5 - 60$ rad/sec. For each maneuver, a sweep amplitude of $\pm 5.0\%$ was used on the swept reference input. Figures 17 and 18 also show time histories of motors δ_{A_2} , δ_{A_4} , δ_{A_6} , and δ_{A_8} , as well as roll rate p and pitch rate q .

During the Tetrad 1 roll sweep (Fig. 36), the frequency sweep reference input r_3 is summed directly into the commands of motor 4 δ_{A_4} and motor 8 δ_{A_8} , which leads to high correlation between those two signals (Fig. 36, third and fifth subplots). In addition, the control system results in correlation of the other two motors shown δ_{A_2} and δ_{A_6} (Fig. 36, second and fourth subplots). The primary response of the aircraft is in roll rate p , with small excursions in pitch rate q .

During the Tetrad 2 pitch sweep (Fig. 37), the frequency sweep reference input r_6 is summed directly into the commands of motor 2 δ_{A_2} and motor 6 δ_{A_6} , which leads to high correlation between those two signals (Fig. 36, second and fourth subplots). The control system results in correlation of the other two motors shown δ_{A_4} and δ_{A_8} (third and fifth subplots, Fig. 36). The primary response of the aircraft is in pitch rate q , with minor excursions in roll rate p .

A quantitative cross-control correlation analysis was performed to confirm the bare-airframe motor input correlation for the Tetrad 1 roll r_3 sweep seen qualitatively from the time histories in Fig. 36. Figure 38 shows the cross-control correlation analysis for the Tetrad 1 roll r_3 sweep between four of the eight bare-airframe motor inputs (primary input δ_{A_4} and secondary inputs δ_{A_2} , δ_{A_6} , and δ_{A_8}). The cross-control coherence (Fig. 38, bottom subplot) is $\gamma_{\delta_1\delta_2}^2 > 0.5$ over a broad frequency range, violating the guideline in Eq. 3. Therefore, traditional conditioning of the responses using the MISO Direct Method identification technique cannot be used in this case due to the inversion of the ill-conditioned matrix in Eq. 2. Furthermore, the secondary inputs cannot be ignored, because their magnitudes are large compared to the primary input magnitude (Fig. 38, top plot) which violates the guideline in Eq. 4.

Figure 39 shows the cross-control correlation analysis for the Tetrad 1 roll r_3 sweep between four of the eight reference signals (primary input r_3 and secondary inputs r_1 , r_2 , and r_4). Here, the cross-control coherence and secondary input magnitudes are all low (meet the guidelines in Eqs. 3 and 4). Therefore, the MISO Direct Method can be applied to the data with the reference signals as the inputs. Then, the JIO Method is applied to post process the results and extract the bare-airframe frequency responses.

Figures 40 and 41 show the identified roll rate p and pitch rate q frequency responses to motors 2, 4, 6, and 8. Although there is no truth model to compare against in this case, several observations can be made to validate these results:

1. All identified frequency responses have high coherence ($\gamma_{xy}^2 > 0.6$) across a broad frequency range.
2. Due to XZ-plane symmetry of the octocopter configuration, the roll rate p response to motors 2 and 6 are of equal magnitude but opposite sign (i.e., off by -180 deg in phase) (Fig. 40) as expected. This is also the case for the roll rate p response to motors 4 and 8.
3. The roll rate response to motor 2 p/δ_{A_2} is about 8 dB (2.5 times) smaller than the roll rate response to motor 4 p/δ_{A_4} (Fig. 40). This is consistent with the larger moment arm from the axis of symmetry

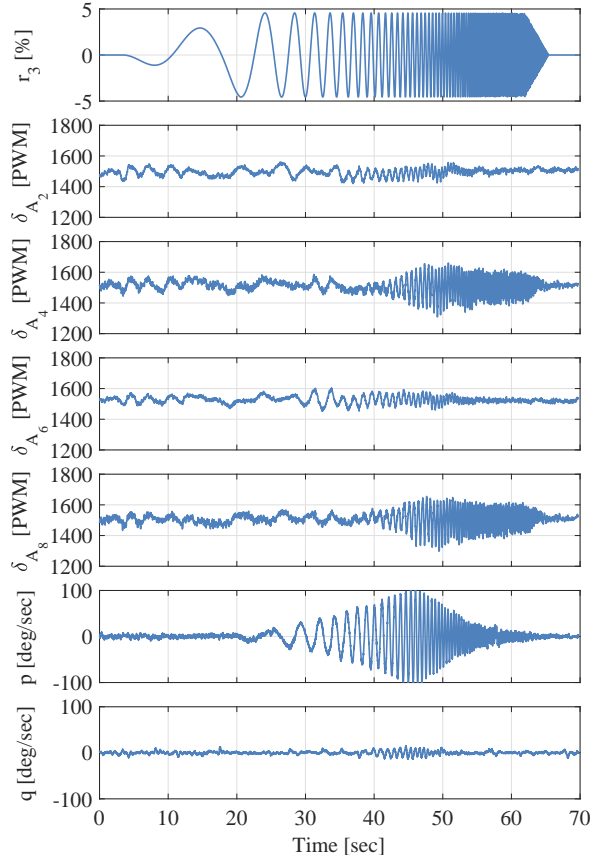


Figure 36. Closed-loop Tetrads 1 roll frequency sweeps (Octocopter flight-test example).

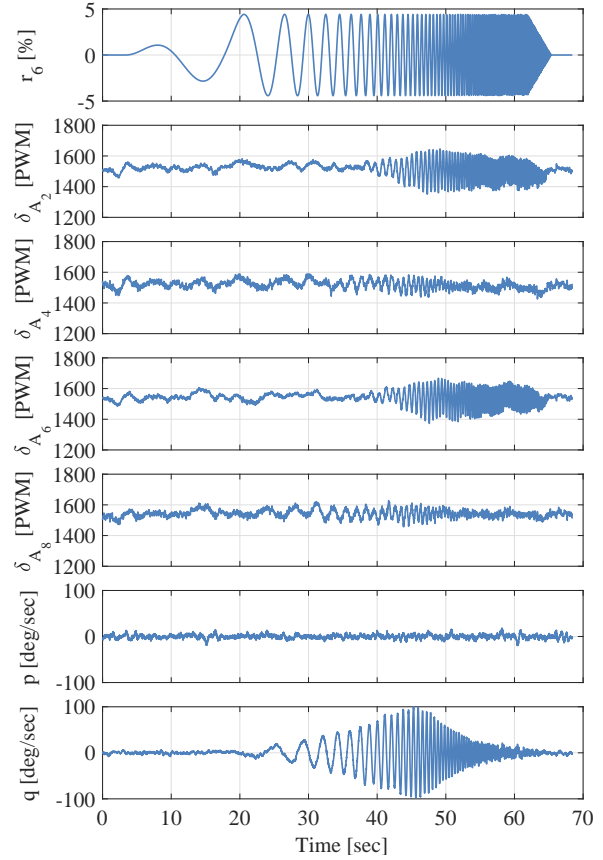


Figure 37. Closed-loop Tetrads 2 pitch frequency sweeps (Octocopter flight-test example).

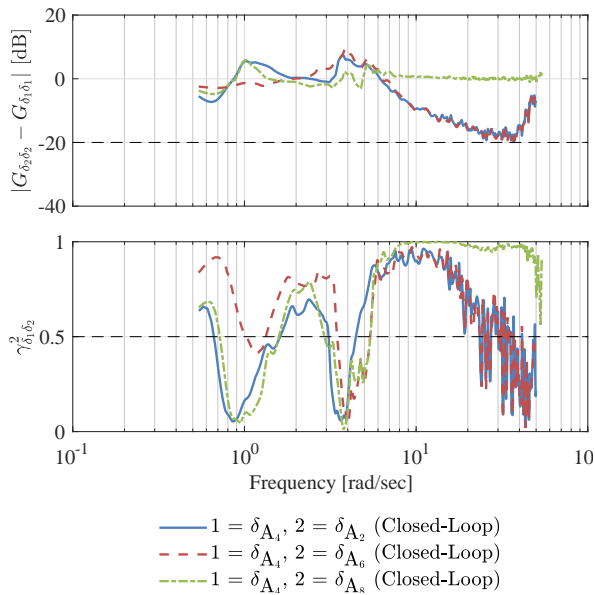


Figure 38. Closed-loop Tetrads 1 roll frequency sweep cross-control correlation for motor inputs (Octocopter flight-test example).

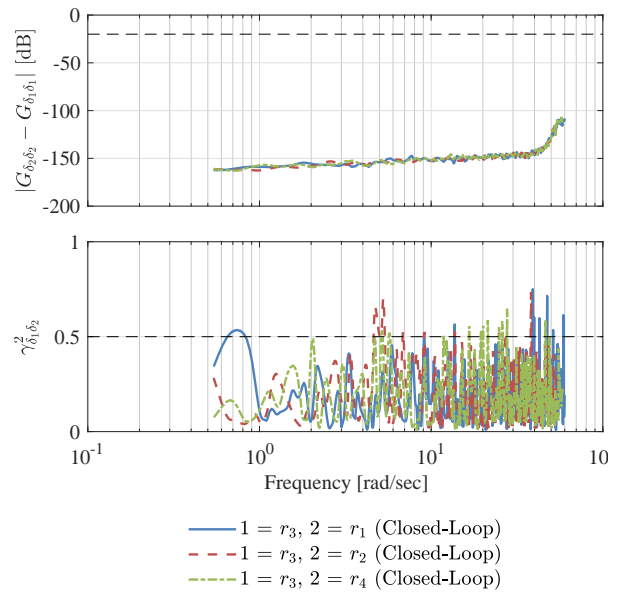


Figure 39. Closed-loop Tetrads 1 roll frequency sweep cross-control correlation for reference inputs (Octocopter flight-test example).

of motor 4 as compared to motor 2:

$$\frac{\sin(112.5 \text{ deg})}{\sin(22.5 \text{ deg})} = 2.4 \quad (18)$$

This is also the case for the roll rate p response to motors 6 and 8.

4. Similar observations can be made about the pitch rate q response to motors 2, 4, 6, and 8 (Fig. 41).
5. Due to the near YZ-plane symmetry of the octocopter configuration, the roll rate response to motor 4 p/δ_{A_4} (Fig. 40, dashed red line) is similar to the pitch rate response to motor 6 q/δ_{A_6} (Fig. 41, dashed green line). This is also the case for the following pairs:

$$\frac{p}{\delta_{A_2}} \approx \frac{q}{\delta_{A_4}}, \quad \frac{p}{\delta_{A_6}} \approx \frac{q}{\delta_{A_8}}, \quad \frac{p}{\delta_{A_8}} \approx \frac{q}{\delta_{A_2}} \quad (19)$$

These results show that it is possible to identify the octocopter frequency responses to individual motors from flight-test data with highly-correlated motor signals. These accurate frequency response identification results are the basis for the parametric reconfigurable multirotor model of Ref. 19.

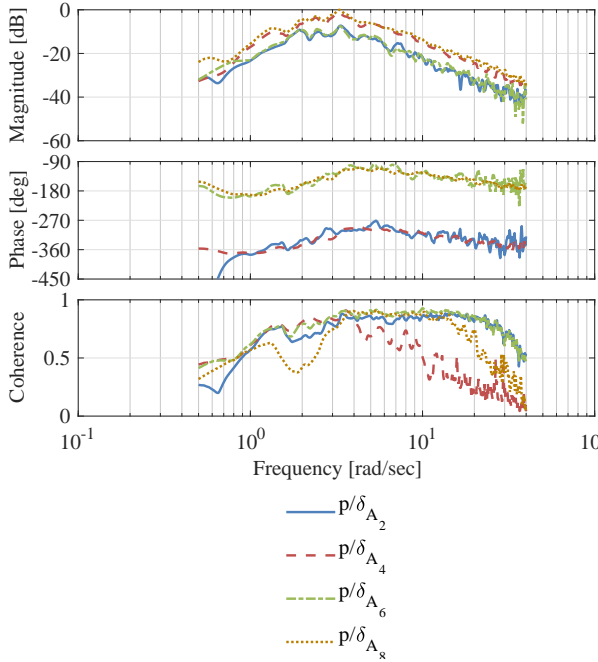


Figure 40. Roll rate to motors 2, 4, 6, and 8 frequency response comparison (Octocopter flight-test example).

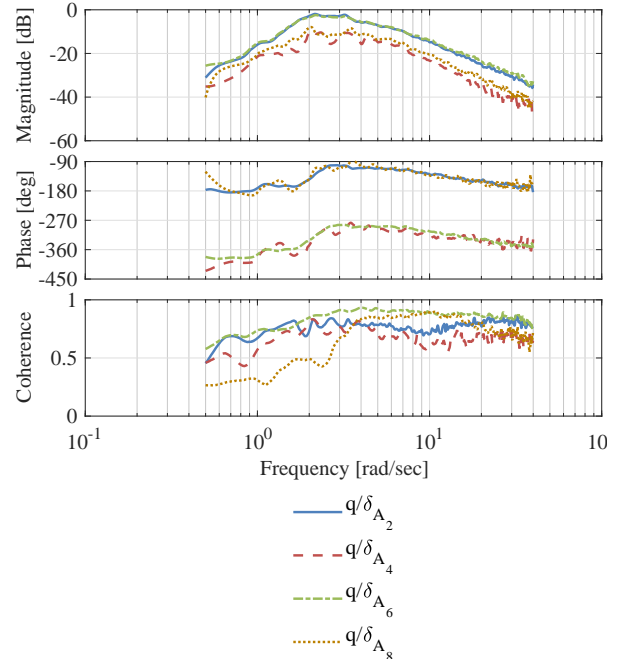


Figure 41. Pitch rate to motors 2, 4, 6, and 8 frequency response comparison (Octocopter flight-test example).

V. Conclusions

The Joint Input-Output (JIO) Method was presented as a way of extracting frequency responses of a multi-input/multi-output (MIMO) system with highly-correlated inputs. The method relies on treating both the input and output of the MIMO system as output to reference inputs that are at most only partially correlated. Based on the examples presented in this paper, the following conclusions can be reached:

1. The JIO Method was used to extract bare-airframe frequency responses of a business jet and compound rotorcraft from simulation data. Frequency responses extracted from closed-loop simulation data with highly-correlated bare-airframe inputs using the JIO Method showed near perfect agreement with the known bare-airframe models. This validates the JIO Method's ability to extract accurate MIMO bare-airframe frequency response matrices from data with highly-correlated bare-airframe inputs.
2. The closed-loop business jet simulation model was excited by summing simultaneous orthogonal multisine inputs to the actuator commands. The resulting data were processed using the Orthogonal

Discrete Fourier Transform (DFT) Method. Even though the correlation coefficient of the total measured actuator positions were well below the threshold typically used as an upper limit for allowable correlation of explanatory variables,² the DFT Method produced incorrect results when a control system was present that fed back discrete frequencies from one input to the second input as a result of lateral/directional bare-airframe coupling.

3. The JIO Method was used to extract bare-airframe frequency responses of a business jet from flight-test data. Responses extracted from closed-loop flight data with highly-correlated bare-airframe inputs using the JIO Method showed excellent agreement with bare-airframe frequency responses extracted from open-loop flight data with uncorrelated bare-airframe inputs using the Multi-Input/Single-Output (MISO) Direct Method. This demonstrates that the JIO Method works well on real data when noise and disturbances are present.
4. The JIO Method was used to extract bare-airframe frequency responses of an octocopter UAV to individual motor inputs. Roll and pitch rate frequency responses to individual motors matched the expected behavior based on motor moment arms and vehicle symmetry.
5. The JIO Method is a post-processing step on the frequency responses already being determined in the frequency response identification method.

References

- ¹Tischler, M. B. and Remple, R. K., *Aircraft and Rotorcraft System Identification: Engineering Methods and Flight Test Examples Second Edition*, AIAA, 2012, doi: 10.2514/4.868207.
- ²Morelli, E. and Klein, V., *Aircraft System Identification - Theory and Practice, 2nd Edition*, Sunflyte Enterprises, 2016.
- ³Zivan, L. and Tischler, M. B., "Development of a Full Flight Envelope Helicopter Simulation Using System Identification," *Journal of the American Helicopter Society*, Volume 55, Number 2, pp. 22003, April 2010, doi: 10.4050/JAHS.55.022003.
- ⁴Grauer, J. and Morelli, E., "Method for Real-Time Frequency Response and Uncertainty Estimation," *Journal of Guidance, Navigation, and Control*, Vol. 37, No. 1, pp. 336-343, January-February 2014, doi: 10.2514/1.60795.
- ⁵Jung, S., Shim, D. H., and Kim, E.-T., "Helicopter Dynamic Model Identification by Conditional Attitude Hold Logic," *AIAA Paper 2017-1251*, January 2017, doi: 10.2514/6.2017-1251.
- ⁶Forsell, U. and Ljung, L., "Closed-Loop Identification Revisited," *Automatica*, 35(7): 1215-1241, July 1999, doi: 10.1016/S0005-1098(99)00022-9.
- ⁷Akaike, H., "Some Problems in the Application of the Cross-Spectral Method," in *Spectral Analysis of Time Series* (ed. B. Harris), 81-107, John Wiley, New York, 1967.
- ⁸Gennaretti, M., Gori, R., Serafini, J., Cardito, F., and Bernardini, G., "Identification of Rotor Wake Inflow Finite-State Models for Flight Dynamics Simulations," *CEAS Aeronautical Journal*, Vol. 8, (1), pp. 209230, March 2017, doi: 10.1007/s13272-016-0235-y.
- ⁹Hersey, S., Celi, R., Juhasz, O., Tischler, M. B., Rand, O., and Khromov, V., "State-Space Inflow Model Identification and Flight Dynamics Coupling for an Advanced Coaxial Rotorcraft Configuration," presented at the American Helicopter Society 73rd Annual Forum, Fort Worth, TX, May 2017.
- ¹⁰Knapp, M. E., Berger, T., Tischler, M. B., and Cotting, M. C., "Development of a Full Envelope Flight Identified F-16 Simulation Model," *AIAA Paper 2018-0525*, January 2018, doi: 10.2514/6.2018-0525.
- ¹¹Berger, T., Tischler, M. B., Hagerott, S. G., Cotting, M. C., Gresham, J. L., George, J. E., Krogh, K. J., D'Argenio, A., and Howland, J. D., "Development and Validation of a Flight Identified Business Jet Simulation Model Using a Stitching Architecture," *AIAA Paper 2017-1550*, January 2017, doi: 10.2514/6.2017-1550.
- ¹²Tischler, M. B., Berger, T., Ivler, C. M., Mansur, M. H., Cheung, K. K., and Soong, J. Y., *Practical Methods for Aircraft and Rotorcraft Flight Control Design: An Optimization-Based Approach*, AIAA, 2017, doi: 10.2514/4.104435.
- ¹³Morelli, E. A. and Smith, M. S., "Real-Time Dynamic Modeling: Data Information Requirements and Flight-Test Results," *Journal of Aircraft*, Vol. 46, No. 1, pp. 1894-1905, November-December 2009, doi: 10.2514/1.40764.
- ¹⁴Tischler, M. B., Ivler, C. M., and Berger, T., "Comment on 'Method for Real-Time Frequency Response and Uncertainty Estimation'," *Journal of Guidance, Control, and Dynamics*, Volume 38, Number 3, pp. 547-549, April 2015, doi: 10.2514/1.G000780.
- ¹⁵Berger, T., Juhasz, O., Lopez, M. J. S., Tischler, M. B., and Horn, J. F., "Modeling and Control of Lift Offset Coaxial and Tiltrotor Rotorcraft," 44th European Rotorcraft Forum Proceedings, September 2018, Delft, The Netherlands.
- ¹⁶Berger, T., Tischler, M. B., Hagerott, S. G., Gangsaas, D., and Saeed, N., "Lateral/Directional Control Law Design and Handling Qualities Optimization for a Business Jet Flight Control System," *AIAA Paper 2013-4506*, August 2013, doi: 10.2514/6.2013-4506.
- ¹⁷Berger, T., Tischler, M. B., Hagerott, S. G., Cotting, M. C., Gresham, J. L., George, J. E., Krogh, K. J., D'Argenio, A., and Howland, J. D., "Handling Qualities Flight Test Assessment of a Business Jet $N_z U P$ - β Fly-By-Wire Control System," *AIAA Paper 2017-1398*, January 2017, doi: 10.2514/6.2017-1398.
- ¹⁸Gong, A., Hess, R., and Tischler, M., "Frequency Domain System Identification and Model Stitching of a Package-Delivery Octocopter," presented at AIAA SciTech, January 2019, San Diego, CA.

¹⁹Lopez, M. J. S., Tischler, M. B., Juhasz, O., Gong, A., Sanders, F. C., and Walan, A. M. G., “Development of a Reconfigurable Multicopter Flight Dynamics Model from Flight Data Using System Identification,” to be presented at the 8th Biennial Autonomous VTOL Technical Meeting, January 2019, Mesa, AZ.